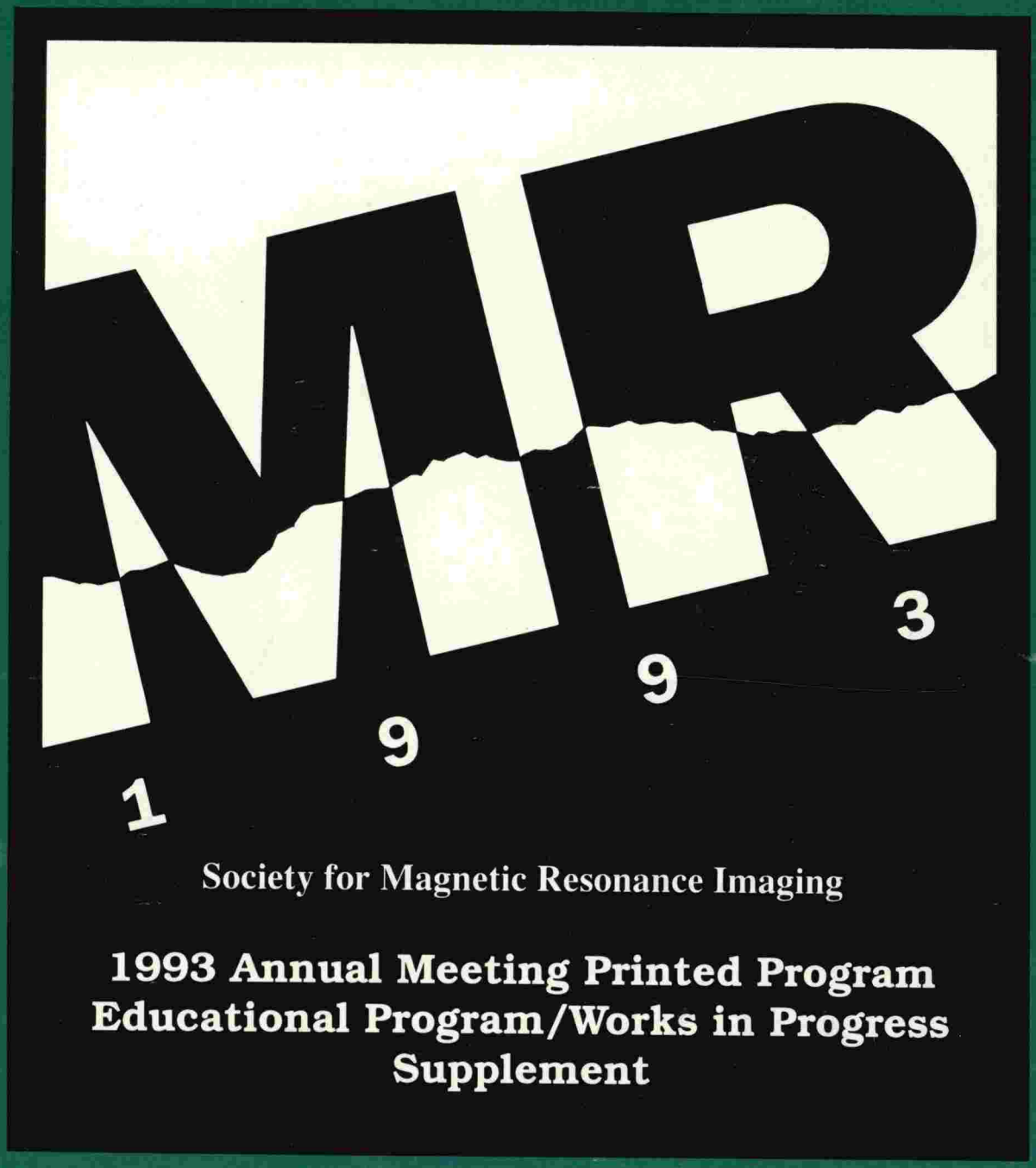

Society for Magnetic Resonance Imaging

1993 Annual Meeting Printed Program
Educational Program/Works in Progress
Supplement

JMRI Journal of Magnetic Resonance Imaging

Table of Contents

MR 1993

Letter from the President

The **SMRI** welcomes you to the 1993 Annual Meeting in San Francisco. The 11th Anniversary Meeting of the **SMRI** begins with the traditional Educational Program on Saturday, March 27 and extends to Monday, March 29. The weekend Educational Program provides an excellent faculty group covering all aspects of clinical MR, while the Monday Economic Symposium addresses all aspects of the quality and cost of MR scanning. Abstracts of the Educational Program plenary talks are included in this supplement.

The Scientific Program Committee has organized a strong and comprehensive program for San Francisco. Introduced by Plenary Sessions presented by experts in the field, the 1993 Works in Progress Program will present 30 presentations, Monday, March 29 – Wednesday, March 31 during the Scientific Program parallel sessions (abstracts are included in this supplement). Each year the Scientific Program Committee is faced with the difficult task of selecting abstracts to construct a well balanced program within the time limitations available. This, coupled with space limitations imposed on the entire Poster Program, regrettably forced the Organizing Committee to reject many strong submissions. Space restrictions, luckily, will not be a factor in planning the 1994 Program.

To complement the educational and scientific programming scheduled, the Technical Exhibits Area will provide access to the latest in MR equipment and accessories. Start your review of the exhibit area with the Technical Exhibits Opening Reception on Saturday, March 27 (5:00 PM-7:00PM). Works in Progress poster presentations are again included in the Scientific Program and are displayed adjacent to the Technical Exhibits Area. Posters may be viewed daily from 8:00 AM-8:00 PM or, more leisurely, during the daily discussion period over the luncheon hour. In addition, you may review award winning posters during the Poster Exhibit Reception, scheduled on Sunday, March 28, (5:00 PM-7:00 PM). The **SMRI** Gala Reception will be held on Monday, March 29 (7:30 PM-10:30 PM). As usual, these receptions will provide you with an opportunity to formally visit and share information with your colleagues.

The **Journal of Magnetic Resonance Imaging**, launched in 1991 by the **SMRI**, has become a major force in the dissemination of information in our field. We encourage you to submit your clinical and technical papers to **JMRI**. The journal will occupy booth #902 where papers may be submitted for consideration.

The **SMRI** looks forward to the most exciting and rewarding Annual Meeting ever!

Sincerely,

Steven E Harms, MD
SMRI *President*

SAT 3/27

8:00 AM - 10:00 AM
Introduction to MRI Scanning
Moderator: J P Keller, PhD

Intro to MRI: Show and Tell.....P L Davis, MD
How to Diagnose & Resolve
Imaging Problems.....J P Keller, PhD
Protocol and Technique.....E K Fram, MD
FAST Imaging.....S W Atlas, MD

10:00 AM - 10:30 AM
Break.....Ballroom Foyer

10:30 AM - 12:00 PM
Brain Diagnostics I
Moderator: W T C Yuh, MD, MSEE

Brain Tumor.....R N Bryan, MD
Sellar, Parasellar,
and Skull Base.....W G Bradley, Jr, MD, PhD
MR of Stroke.....W T C Yuh, MD, MSEE

12:00 PM - 1:30 PM
Luncheon.....Franciscan and Imperial Ballrooms

1:30 PM - 3:00 PM
Brain Diagnostics II
Moderator: R B Lufkin, MD

White Matter Disease
and Miscellaneous.....B P Drayer, MD
Congenital Brain Disease.....W S Ball, MD
Head and Neck.....R B Lufkin, MD

3:00 PM - 3:30 PM
Break.....Ballroom Foyer

3:30 PM - 5:00 PM
Spine Diagnostics
Moderator: G D Sze, MD

Tumor of the Spine.....G K Sze, MD
Degenerative Disk Disease.....J S Ross, MD
Congenital Spine Disease.....A J Barkovich, MD

SMRI '93 Eleventh Annual Meeting

Educational Program Abstracts

Saturday Morning ▪ Plaza Ballroom
Educational Program ▪ EP001–EP004

Introduction to MRI Scanning

8:00 am—10:00 AM
Moderator: J P Keller, PhD

EP001 ▪ 8:00 AM

Introduction to MRI: It's All Done With Magnetic Fields

Peter L Davis, MD
Pittsburgh NMR Institute
Department of Radiology

The basic principles of electromagnetism that are used to generate and transmit electricity are the same principles on which the physics of MRI are based. These principles can be easily demonstrated and will be demonstrated with models at this presentation. Only two basic principles of electromagnetism need to be explained. First, an electrical current produces a magnetic field. Second, a changing magnetic field induces or generates an electrical current in a conductor. Each of these principles will be explained in detail and its application to MRI demonstrated.

A current is a set of moving charges. These charges can be either positive or negative. In a wire it is the negative charge associated with the electrons that move. In the proton, which spins, it is the positive charge which is distributed throughout the proton that is the current. This current produces the magnetic field of the proton. The proton's magnetic field can be attracted or repelled by other magnetic fields in the same way that two bar magnets will attract or repel each other depending on the orientation of their magnetic fields. Therefore, magnetic fields can be used to align the proton and to angulate it.

Since the proton acts as though it is spinning, it also has the property of angular momentum. If an accessory magnetic field, the radio frequency magnetic field, is used to tilt the proton from its initial orientation with the main magnetic field, as the main magnetic field attempts to realign the proton, the proton will wobble or precess like a top. As the proton precesses, its magnetic field also precesses. This precessing magnetic field is a changing magnetic field with respect to a conductor. Therefore, by the second principle of electromagnetism that a changing magnetic field induces an electrical current in a conductor, the precessing magnetic field of the proton will induce an electrical current in a conductor, in this situation the radio antenna or coil of the MRI equipment. This electrical current is the received MRI signal.

EP002 ▪ 8:30 AM

Image Optimization in MRI

Paul J Keller, PhD
Barrow Neurological Institute
Magnetic Resonance Research

Suppose that you scanned a patient and were displeased with the image quality, the images were grainy meaning low SNR. You decide to repeat the scan with different parameters to improve SNR. What do you change? The TR could be increased to allow more recovery of longitudinal magnetization between each excitation, or the TE could be shortened to decrease the decay of transverse magnetization. However either of these modifications would also change the image contrast. This leads to a comparison of apples to oranges! In order to avoid this situation, the relationship between SNR, spatial resolution and scan time will be reviewed holding contrast constant.

SNR may be improved independent of resolution by signal averaging (increasing the number of excitations per phase encoding step, or NEX) — the cost here is scan time. This is not an even trade. Doubling the scan tirne does not double SNR, but yields an increase of only the square root of 2 ~ 1.4. The silver lining here is that cutting the scan time by a factor of 2 does not cut SNR by 2, but by root 2! This is very useful to keep in mind with un-cooperative patients.

In general the relationship between SNR and resolution is an even trade; one of these may always be improved at the expense of the other. This may be best understood through the concept of a voxel. A voxel is that volume element in the body which corresponds to one picture element in the image. Any parameter change which makes voxels smaller improves resolution at the cost of SNR. Conversely, larger voxels improve SNR but decrease resolution. We view this as an even trade. For example if voxel size is decreased by a factor of 2, resolution increases by a factor of 2 and SNR decreases by a factor of 2.

The dimensions of this rectangular solid that is a voxel are: slice thickness x (FOV . # of phase encoding steps) x (FOV . # of frequency encoding steFs). Clearly, the parameters at hand for changing voxel size are slice thickness, FOV and matrix size. Decreasing slice thickness by a factor 2, decreases voxel size by a factor of 2, thus doubling the resolution and halving SNR. Decreasing the FOV by a factor of 2 cuts voxel size by a factor of 4 (factor of 2 in each of two dimensions), yielding 4 times the resolution but one fourth of the SNR! Decreasing FOV can rapidly lead to unacceptably noisy images.

SNR is proportional to the square root of all of the sampled points (# of frequency encoding points x # of phase encoding steps x # of slices(3D only) x NEX). With this in mind consider what happens when the # of phase

encoding steps is doubled, but the FOV stays the same. Voxel size is cut in half in the phase dimension, thus doubling resolution. Considering the change in voxel size alone, one would expect to lose a factor of two in SNR. However, since the # of phase encoding steps is doubled this buys back a factor of root 2 in SNR. The net result is a loss of only root 2 in SNR.

In volumetric or 3D scanning every excitation yields signal from all of the slices, which explains why SNR is proportional to the number of slices. Indeed it can be argued that no more than one NEX should be used for 3D. Instead of doubling the NEX, double the # of slices (same thickness) — the SNR improvement is the same, even if the additional slices are outside the anatomy! Another benefit of this scheme is that any slice dimension wrap around falls in slices which are not of interest.

Finally, SNR is also dependent on the receiver bandwidth. The bandwidth is the range of frequencies that will properly be detected by the receiver. Decreasing this bandwidth by a factor of 4 doubles SNR, while voxel size is unchanged. As you might suspect, there is no free lunch or SNR. The pixel-to pixel frequency discrimination in the image suffers. The image miss-registration between fat and water increases with decreased receiver bandwidth. In fact anv uncontrolled variation in resonance frequency due to inhomogeneity, metal, or gradient non-linearity gives rise to spatial miss-mapping, which is exacerbated by decreasing the bandwidth.

EP003 ▪ 9:00 AM

Techniques and Protocols

Evan K Fram, MD
Barrow Neurological Institute, St. Joseph's Hospital

An overview of MRI imaging techniques will be presented, including the following topics: image contrast, image formation, image acquisition techniques, and presaturation techniques. The interaction between intrinsic tissue parameters and MR pulse sequence parameters determines image contrast. Important intrinsic tissue parameters are proton density, T1 relaxation time, T2 relaxation time, chemical shift, flow (movement), and bound/unbound water content. Important pulse sequence parameters include repetition time (TR), echo time (TE), flip angle, and echo formation technique (spin echo vs. gradient echo). Manipulation of pulse sequence parameters controls the contribution of each intrinsic tissue parameter to image contrast.

Basic features of image formation in MRI are slice selection, frequency encoding, and phase encoding. Reducing receiver bandwidth during frequency encoding allows significant improvement in SNR without prolonging acquisition time. However, chemical shift artifact and minimum echo time increase, requiring selected use of this technique. The image acquisition technique, the sequence in which slices are excited, affects not only acquisition efficiency and SNR, but also affects contrast in the presence of flow. Four commonly used acquisition techniques will be described: single slice (sequential slice), multislice, volume (3DFT), and MOTSA (multiple overlapping, thin slab acquisition).

Presaturation pulses are additional rf pulses applied immediately before the normal excitation pulse. By selectively exciting tissues based on their location or intrinsic MR characteristics, presaturation pulses can selectively suppress signal from the targeted tissues.

Spatial presaturation pulses are commonly used in two situations. First, they can be used to suppress signal from a region on of the body that may contribute artffact to a region of interest. For example, spatial presaturation pulses applied to the anterior soft tissues of the abdomin, chest, or neck reduce signal and therefore phase encoding artifact from these regions that would otherwise project over the spine (the region of interest). Second, spatial presaturation pulses are used in MRA to eliminate signal within vessels based on direction of flow. In neck MRA, for example, superiorly placed presaturation pulses eliminate signal from inferiorly flowing blood within veins without affecting superiorly flowing blood within the carotid and vertebral arteries.

Chemical shift selective excitation pulses are used in post-gadolinium T1 weighted images. Enhancing tissues within fat containing regions, e.g. orbit and bone marrow, may become isointense with fat, making them inconspicuous. Chemical shift selective fat suppression can be used to suppress signal from fat, allowing easy differentiation between high signal intensity fat and other tissues with short T1, enhancing tissue and subacute hemorrhage.

Magnetization transfer presaturation can be used to suppress tissues with relatively large amounts of bound water without affecting tissues with little bound water. For example, magnetization transfer presaturation can be used in brain MRA to improve contrast between brain (suppressed due to bound water) and blood (unaffected because of little bound water) using a mechanism unrelated to flow.

EP004 ▪ 9:30 AM

Fast Imaging:
Principles and Clinical Applications in the CNS*

Scott W Atlas, MD
Neuroradiology Section
Department of Radiology
Hospital of the University of Pennsylvania

*excerpted from "Fast Imaging: Principles, Techniques, and Clinical Applications", Wehrli, F.W., and Atlas, S.W., pages 1013-1078; in: Magnetic Resonance Imaging of the Brain and Spine, S.W. Atlas, editor, Raven Press, New York, 1991.

The archetype of scanning techniques which shorten acquisition times is one known as *gradient echo imaging*, a generic term which appropriately has come to represent an entire family of pulse sequences. The variety of different sequences encompassed by this title generally share two major features, which distinguish gradient echo scanning from the more traditional counterpart of spin echo imaging: 1) the radiofrequency (RF) excitation pulse, or flip angle, is operator-dependent, and in fact is generally less than the 90° pulse of the spin echo sequence, and 2) signal is acquired by virtue of reversal of the read-out (frequency-encoding) gradient in the absence of the 180° refocussing RF pulse of spin echo scanning. These two features, although quite straightforward, have profound implications with regard to image contrast and specific image characteristics found in gradient echo images. The current role of the various fast

imaging techniques using 2DFT and 3DFT gradient echo acquisition in the clinical assessment of the brain and spine can be divided into three general categories: 1) the detection of vascular lesions and flow, 2) the depiction of areas of abnormal magnetic susceptibility, and 3) the evaluation of extramedullary spinal disease.

An alternative method of reducing scan time in any MR sequence can be found in nontraditional approaches to traversing k-space. One such fast imaging scheme (fast spin echo) involves a hybrid approach to reducing acquisition time; that is, combining the rf refocussing of a CPMG sequence with the acquisition of multiple lines (i.e. discontinuous regions) of k-space during a single TR. This technique results in contrast characteristics similar to those of conventional long TR spin echo images, with the notable exception of decreased magnetic susceptibility-induced hypointensity in regions of brain iron and intracranial hemorrhage. The potential benefits of fast spin echo imaging are clear: increased patient throughput, reduction in patient motion problems, and potential implementation of very high resolution imaging in reasonable time frames.

Saturday Morning ▪ Plaza Ballroom
Educational Program ▪ EP005–EP007

Brain Diagnostics I

10:30 AM-12:00 PM
Moderator: W T C Yuh, MD, MSEE

EP005 ▪ 10:30 AM

Magnetic Resonance Imaging of Brain Tumors

R Nick Bryan, MD, PhD
Johns Hopkins Hospital
Department of Neuroradiology

I. Pathologic Types of Brain Tumors
  A. Primary
    1. Glial Origin
      a) Pathologic Grade
        (1) Kernohan Classification
          (a) Grade 1-Benign
          (b) Grade II-Anaplastic
          (c) Grade III and IV-Glioblastoma
      b) Cell Type
        (1) Astrocytoma
        (a) Pilocytic
          (b) Giant Cell
          (c) Pleomorphic Xanthoastrocytoma
        (2) Oligodendroglioma
        (3) Ependymoma
        (4) Pinealoma
        (5) Choroid Cell Papilloma
        (6) Ganglioglioma
    2. Meningeal
      a) Meningioma
      b) Hemangiopericytoma
    3. Nerve Sheath Tumors
      a) Cranial Nerve Neuroma
    4. Vascular Tumors
      a) Hemangioblastoma
    5. Primitive Neuroectodermal Tumor (PNET)
      a) Medulloblastoma
      b) Dysgerminoma
    6. Craniopharyngioma
    7. Dermoid/Epidermoid
    8. Primary CNS Lymphoma
  B. Secondary
    1. Hematogenous
    2. CSF Seeding

II. Distinguishing Features of Brain Tumors
  A. Age of Patient
  B. Number of Lesions
  C. Anatomic Location
    1. Intraaxial/Extraaxial
    2. Supratentorial/Infratentorial
    3. Cortical/Subcortical
    4. Intra or paraventricular
    5. Suprasellar
    6. Pineal Region
    7. CPA
  D. Imaging Features
    1. Margination
    2. "Fluid" Component
    3. Hemorrhagic Component
    4. Contrast Enhancement

EP006 ▪ 11:00 AM

MR of the Sella, Parasellar Region, and Skull Base

William G Bradley, Jr, MD, PhD
Memorial Medical Center of Long Beach
Memorial Magnetic Resonance Center

Magnetic resonance imaging (MRI) is the imaging modality of choice for the evaluation of suspected pituitary adenomas. Most functioning pituitary adenomas are microadenomas (ie, less than 1 cm in height) and 80% of all microadenomas are prolactinomas. The classic prolactinoma appears as a laterally-positioned hypointensity which enhances less than the normal gland following administration of Gadolinium. If the prolactin level is "definitely" elevated (greater than 100 ng/ml) then there is no need to administer Gadolinium as the referring clinician will probably treat with bromocriptine anyway. When the prolactin level is elevated over 1000 ng/ml, cavernous sinus invasion is usually present (which can be very difficult to determine by MR). Macroadenomas present by mass effect on the chiasm, classically with a bitemporal hemianopsia. Typically, such lesions have a waist as they pass through the diaphragma sellae. If the waist is particularly narrow, the tumor may not be resectable through a transsphenoidal approach. The primary differential diagnoses for pituitary macroadenomas are meningioma and aneurysm. Meningiomas tend to narrow the carotid artery when they invade the cavernous sinus while macroadenomas tend to surround it without narrowing. While both tumors enhance with contrast, meningiomas have a typical "dural tail". Aneurysms of the distal internal carotid artery or basilar artery generally contain blood breakdown products (eg, methemoglobin) and have a flow void. Macroadenomas tend to obliterate the "bright spot" of the posterior lobe (which is still seen with craniopharyngiomas, Rathke's cleft cysts, hamartomas of the tuber cinereum, and gliomas of the optic nerve, chiasm and hypothalamus).

At the skull base, schwannomas of the cranial nerves are best detected with thin T1weighted images before and after administration of Gadolinium. Acoustic neurinomas generally extend into the porus acousticus while

meningiomas tend not to. Approximately 5% of acoustic neurinomas are associated with arachnoid cysts. Schwannomas of the trigeminal nerve typically have a dumbbell appearance, producing masses in the cavernous sinus and in the pontine cistern. Other skull base lesions to be considered in the differential diagnosis include chordomas (originating from the clivus), chondrosarcomas, and contiguous spread of squamous cell carcinoma or adenocystic carcinoma along the branches of the trigeminal nerve as it passes through the foramen rotundum or foramen ovale into the cavernous sinus and Meckel's cave, respectively. Other extraaxial masses in this area include aneurysms of the PICAs or vertebral arteries and epidermoid tumors.

References:
Hasso AN, Hinshaw DB, Kief-Garcia ML Chapter 27 "Neoplams of the Cranial Nerves and Skull Base" and Hasso AN, Kortman KE, Bradley WG. Chapter 25 "Supratentorial Neoplasms" both in Magnetic Resonance Imaging 2nd Edition, Mosby-Yearbook, St. Louis, MO 1992.

EP007 ▪ 11:30 AM

MR of Stroke

Wm T C Yuh, MD, MSEE
University of Iowa Hospital and Clinic
Department of Radiology

Stroke with arterial or venous origin is a frequent working diagnosis for patients undergoing MR examinations. Because 20% to 40% of the patients presented with stroke-like symptoms are not caused by arterial or venous occlusive disease, a clear understanding of the patterns of MR findings related to the stroke and its prognostic significance is essential to facilitate a correct diagnosis and exclude other pathological processes. With the introduction of the new neuroprotective and endovascular thrombolytic procedures, early diagnosis of stroke is paramount to minimize the morbidity and mortality. Approximately 20% to 40% of the CT examinations are negative within the first 24 hours in patients with acute stroke. The awareness of the MR finding particularly within the first few hours is therefore essential for the optimal management of the patient.

Specific emphasis:

1. Arterial occlusive disease
   a. Early findings (<24 hour) of acute ischemia
   b. Pattern of MR findings and its prognostic value
   c. Correlation of MR findings with underlying pathophysiology
2. Venous occlusive disease
   a. Pattern of MR findings and its clinical significance
   b. Correlation of MR findings with underlying pathophysiology
   c. Comparing MR findings of venous with arterial occlusive disease

Brain Diagnostics II

1:30 PM-3:00 PM
Moderator: R B Lufkin, MD

EP008 ▪ 1:30 PM

WHITE MATTER DISEASES

Burton P Drayer, MD
Barrow Neurological Institute
Southwest Neuroimaging

The critical role that MRI plays in the diagnosis of white matter disease is well established. The primary finding in all of these disorders is signal hyperintensity seen best on intermediate- and T2weighted spin-echo images. Diagnostic specificity is achieved by understanding the anatomic distribution and pathologic characteristics of the white matter lesions:

(A) *Demyelinating (Myelinoclastic)*

•***Multiple Sclerosis*** - Sharply defined, perpendicular, periventricular lesions (Dawson's fingers); involvement of peritemporal horn region of middle cerebellar peduncle, corpus callosum inferior surface, arcuate fibers; discrete posterior column and pontine lesions.

•***Ischemic White MatterDisease*** - Multifocal or confluent, often poorly marginated deep cerebral white matter; spares corpus callosum and arcuate fibers; poorly circumscribed basal ganglia and midpontine changes; no posterior column or middle cerebellar peduncle involvement.

•***Radiation Injury*** - Diffuse, sheetlike changes in radiation port; necrosis, enhancement, ± mass effect if radiation necrosis.

•***ADEM***- Recent viral illness, multifocal lesions (± gray matter).

•***Disseminating Necrobzing Leukoencephalopathy (DNL)*** - Severe diffuse demyelination in children receiving methotrexate and radiation therapy.

•***AIDS leukoencephalopathy*** - Multifocal, nonenhancing patches of cerebral white matter involvement.

•***Progressive multifocal leukoencephalopathy (PML)*** - Large, asymmetric nonenhancing foci in setting of immunosuppression.

•***Central pontine and extrapontine myelinolysis (CPM)*** - Central pontine ± deep white matter, corpus callosum.

(B) *Dysmyelinating (Leukodystrophy)*

•***Adrenoleukodystrophy***- Young males, posterior dominance (parieto-occipital, splenium).

•***Alexander's*** - Anterior cerebral white matter dominance, large head.

•***Sudanophilic (e g Pelizaeus-Merzbacher)*** - Diffuse, severe cerebral white matter.

•***Canavans*** - Associated atrophy with rounded ventricles, large head.

•***Metachromatic*** - Most common, aryl sulfatase A, abnormal NCV.

•***Mitochondrial, Aminoaciduria*** - Nonspecific.

EP009 ▪ 2:00 PM

Magnetic Resonance Imaging:
The Value of Imaging Techniques in the Differential Diagnosis Of Congenital Brain Malformations

William S. Ball, MD
Children's Hospital and Medical Center
Department of Radiology

Improved anatomic resolution, the ability to image in multiple projections, and contrast sensitivity based on relaxation characteristics have made MRI the imaging modality of choice in the evaluation of complex congenital malformations of the brain. Anatomical dissection which in the past was performed only by anatomists and pathologists, has now given way to in-vivo dissection with MRI. Unraveling the embryogenesis, timing of the event, and better understanding the effect congenital malformations may have on clinical management are important uses of MRI which are often overlooked. A complete review of the vast array of congenital brain malformations is beyond the scope of this presentation. Where MRI can provide information on CNS malformations that effect patient management and the differentiation of congenital malformations from acquired insults will be emphasized.

For the sake of this discussion, I will refer to any malformations that arise during the process of neurulation, ventral induction, neuronal proliferation, histogenesis, and/or neuronal migration as being congenital in origin. Those patterns of injury that originate in utero within the last trimester or more commonly the direct result of an unknown or known insult. Are they also to be considered congenital by virtue of arising in utero, or should they be separated from congenital malformations as encephaloclastic injury? Congenital anomalies may be part of a diffuse syndrome or may be isolated. Some evidence supports that many isolated malformations are the result of a single in-utero insult leading to injury during a specific time in development. Many other malformations may be linked to a genetic abnormality by their association with syndromes, familial patterns of expression, or other organ system developmental anomalies.

EP010 ▪ 2:30 PM

Interventional MR Imaging

RB Lufkin, MD
UCLA Medical Center
Department of RAdiological Sciences

Many of the advantages of MR that make it such a powerful clincal imaging tool are also valuable during interventional procedures. The lack of ionizing radiation and oblique and multiplanar imaging capabilities are particularly useful during invasive procedures. Perhaps the greatest advantage of MR is the high soft-tissue contrast resolution, which allows the early and sensitive detection of tissue changes during interventional procedures.

One of the first applications of MR imaging-guided procedures has been for fine needle aspirtion cytology. Several approaches are also currently under evaluation for the treatment of pathology with MR guidance. Interstitial laser or RF may be applied to deep tissues to deposit thermal energy in a well-defined fashion, with minimal damage to adjacent structures. This technique has been used for lesions in brain, gasserian ganglia, liver, or the conductive pathway to the heart. Other investigators have already demonstrated the possibility in human studies of MR guided catheter placement for intramural alcohol and chemotherapy injections. Interventional MR imaging is clearly in the early stages of development. While the value of MR-guided aspiration cytology and MR evaluation of deep cerebral electrode implantation has already been confirmed with human clinical studies, the ultimate future role for MR-guided interstitial therapy remains to be defined.

Saturday Afternoon ▪ Plaza Ballroom
Educational program ▪ EP011-EP013

Spine Diagnostics

3:30 PM-5:00 PM
Moderator: G K Sze, MD

EP011 ▪ 3:30 PM

Magnetic Resonance Imaging in the Evaluation of Spinal Tumors

Gordon K Sze, MD
Yale University
Department of Radiology

Extradural Tumors

Unenhanced MR scans are generally superb at delineating extradural tumors, whether primary or secondary. Short TR spin echo sequences are generally adequate for the detection and delineation of lesions. Long TR spin echo, STIR sequences, or gradient echo sequences can help for further evaluation. Fast spin echo sequences initially appear problematic since marrow often appears to remain of high signal. When both spin density and T2-weighted images are examined, however, few lesions are missed.

MR can also be useful in patients with compression fractures of the vertebral bodies in order to differentiate between benign osteoporotic collapse and neoplastic replacement as the cause. In acute cases, an even band of normal high signal marrow with smooth margins may remain adjacent to a band of lower signal within the single vertebral body. This appearance is suggestive of a non-neoplastic deformity.

When gadolinium is given for spinal lesions, enhancement is variable, with some lesions enhancing to isointensity. Nevertheless, contrast can still be useful as an adjunct in 1. characterizing possible epidural tumor, 2. indicating regions of more active tumor for biopsy, 3. outlining areas of cord compression, 4. differentiating disk from tumor. It does not appear to always be accurate in distinguishing diffuse marrow involvement with tumor from marrow that is hypointense for other reasons.

Intradural Extramedullary Tumors

Contrast enhanced MR imaging has become the procedure of choice in all suspected intradural extramedullary

tumors. Primary tumors are usually easily identified. Secondary tumors may not be easily visible without contrast. Results appear to be comparable to myelography and post myelography CT. We have seen cases in which the myelogram and post myelographic CT suggested lesions, generally subtle, which the gadolinium enhanced MR scans did not detect; alternatively, we have also seen cases in which the myelogram and post myelographic CT appeared normal but in which the gadolinium enhanced MR scans proved the diagnosis, most often in cases in which fine tumor coated the cord or nerve roots.

Intramedullary Tumors

Gadolinium enhanced MR imaging has become the procedure of choice for suspected cord tumors. Short TR and long TR spin echo sequences in the sagittal plane have become standard, as have short TR images in the axial or coronal planes. Fast spin echo sequences can replace long TR spin echo sequences. Unlike in the brain, the majority of cord tumors appear to enhance. Therefore, absence of enhancement is suggestive, although not conclusive, of another etiology.

EP012 • 4:00 PM

Degenerative Disk Disease

Jeffrey S Ross, MD
Cleveland Clinic Foundation
Department of Radiology

In a prospective, blinded study in 1986, Modic compared surface-coil MR, CT, and myelography in the evaluation of disk herniation and stenosis. There was an 82.6% agreement between MR and surgical findings for the type and location of the disease. This study also showed an 83% agreement between CT and surgical findings and a 71.8% agreement between myelography and surgery. Canal stenosis, ligamentous hypertrophy, and facet disease were all demonstrated with MRI, with good correlation of the canal size seen by MRI with CT. Similar good correlations have been demonstrated for MR in cervical disk disease.

The abnormal disk may be divided into annular bulge or herniation. An annular bulge is the result of degeneration with a grossly intact annulus, recognized as a general extension of the disk margin beyond the margin of the vertebral end plate. This concept of an annular bulge having an intact annulus has been challenged by Yu et al. They found that large disk bulges were invariably associated with annular tears. This group also defined annular tears into three types: a concentric, fluid-filled space between the annular lamellae; radial tears characterized by rupture of all annular layers; and transverse tears which involve rupture of Sharpey's fibers. Transverse and radial tears were visible on MRI as increased signal intensity on T2-weighted images. Annular tears have been noted to enhance on T1-weighted images following the administration of Gd-DTPA, presumably secondary to the ingrowth of scar tissue into the tear as a consequence of the body's attempt at healing. The reason that annular tears are important is the controversial concept of "diskogenic pain", and its implications concerning the usefulness of discography for its diagnosis. Back pain is thought to occur in some patients without morphologic abnormalities such as herniation or stenosis. This is thought to occur when there is leakage of nuclear material through an annular tear into the epidural space or due to irritation of the nerves associated with scar tissue within the annular tear. This is of considerable interest, since discography has been used as a tool for reproducing the patient's diskogenic pain, and diskectomy has been used to treat the condition.

A protruded disk is herniation of nucleus pulposis through a defect in the annulus fibrosus, producing a focal extension of the disk margin. Some portion of the outer annular fibers remain intact, producing a line of decreased signal intensity outlining the herniated material (especially on T2 weighted images). A disk extrusion is nuclear material herniating through a defect in the annulus into the anterior epidural space, which is no longer bounded by the annulus. However, in contradistinction to a free fragment, it remains attached to the parent disk space via a pedicle of nuclear material. A free fragment or sequestered disk is defined as a herniation through a full thickness defect in the annulus, which is no longer attached to the parent disk space. Free fragments may lie anterior or posterior to the posterior longitudinal ligament or, rarely, intradural. Both extruded disks and free fragments may show increased signal intensity on T2-weighted images. Recognition of a free fragment has definite clinical implications because they can produce misleading clinical signs; they are a contraindication to chymopapain injection or percutaneous diskectomy; and they may require a more extensive surgical procedure if there is migration away from the disk space of origin. Schellinger analysed the MR appearance of 47 patients with free fragments or extruded disks. Disk fragments migrated with approximately equal frequency in the superior and inferior directions. Interestingly, the migrating fragments were dislodged either to the right or left of midline in 94%. This localization appears to be secondary to a sagittally oriented midline septum in the anterior epidural space.

EP013 • 4:30 PM

MR of Congenital Spine Disease

A James Barkovich, MD
University of California, San Francisco
Department of Radiology

Anomalies of the spine can be best understood by understanding the embryology of the spine and analyzing the timing of the injuries that result in the anomalies. Formation of the spinal cord can be divided into four main stages: (1) Formation of the notochord between the developing ectoderm and endoderm; (2) Induction of the neural plate; (3) Closure of the neural plate into a neural tube ("neurulation") and disjunction of the neural plate from adjacent cutaneous ectoderm; and (4) Formation of the caudal spinal cord from the caudal cell mass and degeneration of the caudalmost segments of spinal cord into the filum terminale.

Anomalies of the spine can likewise be divided into four major groups depending upon which of the four major steps goes awry. The MR characteristics of the following groups of anomalies will be discussed.

(1) SPLIT CORD MALFORMATIONS

Split cord malformations are believed to result from splitting of the notochord around abnormal adhesions

between endoderm and ectoderm. Included in this group are diastematomyelia, neural enteric fistulae, and neurenteric cysts.

(2) MALFORMATIONS SECONDARY TO PREMATURE DISJUNCTION OF NEUROECTODERM FROM CUTANEOUS ECTODERM

When neuroectoderm separates prematurely from cutaneous ectoderm, the mesenchyme surrounding the neuroectoderm gains access to the primitive ependyma lining the central canal of the developing cord. For unknown reasons, the mesenchyme then differentiates into fat. Thus, spinal lipomas, lipomyeloceles, and lipomyelomeinigoceles are formed.

(3) MALFORMATIONS RESULTING FROM NONDISJUNCTION OF NEUROECTODERM FROM CUTANEOUS ECTODERM

Nondisjunction of cutaneous ectoderm from neuroectoderm results in continuity of skin with neural structures. Included in this group are myelomeningoceles, myeloceles, and dermal sinuses.

(4) MALFORMATIONS RESULTING FROM ABNORMAL TRANSFORMATION OF THE CAUDAL CELL MASS

In some patients, the caudalmost portion of the spinal cord, that formed from the caudal cell mass, evolves abnormally. The tethered cord syndrome and lumbosacral agenesis are the most common anomalies in this group.

SUN 3/28

8:00 AM - 8:30 AM
Vascular Imaging
Moderator: A N Hasso, MD

CNS.....A N Hasso, MD
Body .....J P Finn, MD

8:30 AM - 10:00 AM
Body MR Diagnostics I
Moderator: P J Fritzsche, MD

Protocol and Technique.....D D Stark, MD
Liver .....M E Bernardino, MD
Kidney, Adrenal & Retroperitoneum.....P J Fritzsche, MD

10:00 AM - 10:30 AM
Break.....Grand Ballroom

10:30 AM - 12:00 PM
Body MR Diagnostics II
Moderator: R J Herfkens, MD

Pelvis.....H Y Kressel, MD
Pediatric Abdomen.....R B Dietrich, MB, ChB
Cardiac and Thoracic Images.....R J Herfkens, MD

12:00 PM - 1:30 PM
Luncheon.....Grand Ballroom

1:30 PM - 3:00 PM
Shoulder MR Imaging
Moderator: J B Kneeland, MD

Shoulder: The Surgeon's Perspective .....M S Shapiro, MD
Shoulder: Instability.....M Rafii, MD
Shoulder: Impingement/Rotator Cuff Disease ...J B Kneeland, MD

3:00 PM - 3:30 PM
Break.....Grand Ballroom

3:30 PM - 5:00 PM
Other Musculoskeletal MR Diagnostics
Moderator: L L Seeger, MD

Knee: Menisci & Cruciates.....L L Seeger, MD
Knee: Non Meniscal Pathology.....J V Crues III, MD
Foot/Ankle .....R M Kerr, MD

Vascular Imaging

8:00 AM-8:30 AM
Moderator: A N Hasso

EP014 ▪ 8:00 AM

Vascular Imaging of the Central Nervous System

Anton N Hasso, MD, FACR
Loma Linda University Medical Center
Department of Radiological Sciences

Extracranial Circulation:

MR angiography (MRA) has been shown to be a useful tool in evaluating patients with cerebral ischemia and stroke. The technique is applicable for demonstrating occlusive diseases in the cervicocranial, intracranial carotid, and vertebrobasilar circulations. Our experience, and that of others, has shown that arterial stenosis can be consistently demonstrated. The extracranial carotid vessels are ideally imaged in the axial projection which maximizes the time-of-flight effects. The 3-D data set can then be viewed in any plane, in addition to the axial plane of acquisition. MRA examinations can be used to demonstrate the whole length of the internal carotid artery from its origin in the neck to its intracranial bifurcation. Two or three stacked axial acquisitions may be necessary for complete evaluation of the carotid artery.

Intracranial Vessels:

The intracranial vessels and their major branches can be depicted by a variety of techniques. Generally, an axial acquisition through the circle of Willis shows the intracranial circulation optimally. Additional coronal and sagittal slabs may be needed to fully define the anterior and posterior cranial circulations. MRA has a role in the evaluation of a variety of intracranial occlusive vascular diseases. Stenoses or occlusions of the intracranial arteries may be identified, provided the vessels are of sufficient caliber.

Depiction of Vascular Lesions:

Time-of-flight MRA can define the circle of Willis sufficiently to allow detection of intracranial aneurysms as small as 3-4 mm in diameter. Aneurysms with slow flow or giant aneurysms that are partially thrombosed are difficult to detect on the projection images alone. A review of the conventional spin echo images and a careful review of the individual partitions may help in the correct diagnosis. The injection of gadolinium will help to detect the slow flow through a giant aneurysm.

MRI has proven to be a good means for detecting and characterizing intracranial arteriovenous malformations (AVMs). MRA techniques can delineate the nidus and major feeding vessels of AVMs without invasive angiography.

Depiction of venous angiomas may be accomplished by MRA. On time-of-flight studies, gadolinium has to be injected in order to see the slowly flowing veins extending through the central cerebral and cerebellar white matter. In one study, 13 of 14 venous angiomas were detected on detailed thin slab acquisitions.

Depiction of Neoplasms:

The depiction of extra- and intracranial neoplasms is improved by various angiographic techniques. Conventional angiograms are utilized to localize lesions and to detect their point of origin. For example, extraaxial tumors will have a different blood supply from intraaxial parenchymal or intraventricular tumors. MRA can play a similar role in the differential diagnosis of cranial neoplasms. The vascular pedicle or point of attachment of a neoplasm is greatly aided by projection images following gadolinium enhancement. Gadolinium enhanced MRA improves lesion conspicuity and is able to determine the relationship of neoplasms to the surrounding vessels.

Displacement of vessels is another use of MRA in tumor evaluation. Lesions of the skull base may displace vessels, without invasion. The direction of displacement can aid in the proper surgical approach and in anticipating the structures as they are surgically identified. If a neoplasm is invading a vascular structure, this can also be clearly depicted on MRA. Such invasion may involve an arterial structure or may involve the dural sinuses. For example, a cavernous sinus meningioma can encase the fixed cavernous portion of the internal carotid artery. Tentorial and convexity meningiomas may cause constriction of the dural sinuses or torcula depending on their size and point of origin.

EP015 ▪ 8:15 AM

Vascular Imaging in the Body

J Paul Finn, MD
New England Deaconess Hospital
Department of Radiology

Initially applied to the head and neck, MR angiographic techniques have progressed rapidly, such that all major blood vessels are now accessible to study. 2-D and 3D time-of-flight and phase-contrast methods have been successfully applied to a wide range of diseases in arteries and veins, and well-defined clinical indications for MR angiography are beginning to emerge.

In the abdomen, accurate assessment of disease involving the portal and systemic veins is possible, and blood flow can be characterized and quantified. The veins of the thorax, pelvis and extremities can be evaluated to a level occasionally surpassing catheter venography. Much progress has been made in arteriographic techniques for the abdomen, thorax and extremities, but the more challenging patterns of blood flow and vascular anatomy in these vessels impose demands on hardware and spatial resolution which as yet are not always met. Several promising techniques have recently been proposed which go a long was towards resolving many of these limitations, but much work remains to be done.

In this session, techniques for vascular imaging in the body will be discussed as well as potential pitfalls and artifacts, and how to recognise and avoid them.

Body MRI Diagnostics I

8:30 AM-10:00 AM
Moderator: P J Fritzsche, MD

EP016 ▪ 8:30 AM

Protocol and Technique for MRI of the Body

David D Stark
University of Massachusetts Medical Center
Department of Radiology

The advent of MRI solved the two great limitations of CT for imaging the CNS and the musculoskeletal system, namely: X-ray beam hardening and poor soft tissue contrast. Furthermore, MRI is inherently well suited for imaging small superficial objects that do not move.

On the other hand, the diagnosis of abdominal (including pelvic) disease presents great challenges to any imaging modality. This large anatomic region is often appears to be symptomatic in diseases actually originating within the thorax, spine, or even the lower extremities.

Abdominal imaging must cover a large anatomic region, including eight (8) separate physiological organ systems and at least eleven (11) individual organs. Anatomic proximity and access via the peritoneal cavity commonly causes secondary involvement of neighboring organs.

MRI of the abdomen in particular and the body as a whole is complicated by various asynchronous physiological motions. The intestine may mask or mimic mass lesions, requiring use of contrast media to label the normal bowel lumen. Ultrasound can use peristaltic motion or administered water as a bowel marker; iodine, barium, or fat are routinely used to enhance CT. Many analagous strategies have had limited success with MRI.

Protocols for body MRI must carefully balance the need for anatomic coverage (FOV and slice number) against acquisition time and patient motion. The multiplicity of organs, tissues, and potential diseases having different MR tissue characteristics renders any single pulse sequence inadequate. Unfortunately, within the practical constraint of a one hour examination, a single set of techniques cannot be defined to optimally image the entire abdomen. However, given clinical information or a specific diagnostic question, efficient and powerful imaging protocols exist and are continually improving.

This lecture will discuss protocol concepts and illustrate how specific techniques may be implemented on machines varying in field strength and other hardware capabilities.

EP017 ▪ 9:00 AM

Michael E Bernardino, MD
Emory University Hospital
Department of Radiology

The liver can be evaluated with magnetic resonance for both focal and diffuse disease. In this course we will deal briefly with proper scanning technique. This usually means at least one T1 and T2 sequence. The use of contrast will be addressed. Primarily, at present, this is intravenous gadolinium. Other MR hepatic specific MR contrast agents will be addressed.

Detection of a lesion is important, however, tissue specificity may be more important. MR has the ability to be specific with certain tumors. Examples of distinguishing characteristics for hemangiomas, focal nodular hyperplasia and some hepatomas will be demonstrated. Examples of overlap of the MR images with other lesions will be discussed.

Diffuse liver disease is another important area for MR evaluation. The use of MR fat suppressed techniques in MR for distinguishing focal fatty infiltration from neoplasms will be shown. Pitfalls of these techniques such as field inhomogenity will be discussed.

Another area of MR use in diffuse liver disease is the patient with hemocromatosis. Iron is a potent T2 relaxer. Thus the livers of such patients are usually black. This may be helpful in detecting a hepatocellular carcinoma. The disease acts as its own contrast agent. Also, following T2 values in patients with hemocromatosis correlates extremely well with the amount of iron in the liver and may obviate the need for repetitive biopsies patients on either phlebotomy or penicillamine therapy. In order to obtain accurate data, short TR/TE sequences which have less noise should be used.

EP018 ▪ 9:30 AM

Kidney, Adrenal and Retroperitoneum

Peggy J Fritzsche, MD, FACR
Riverside MRI Center

Magnetic resonance (MR) imaging is assuming an increasingly valuable role in the retroperitoneum because of developments in MR technology. Well known advantages of MRI; include, direct multiplanar visualization of structures, determination of tumor origin and local extension, evaluation of vascular integrity, characterization of lesions, and evaluation of patients with a contra-indication to iodinated contrast material. Motion suppression techniques, flow compensation, presaturation pulses and fast imaging now contribute to diagnostic detail not previously possible.

Since the abdominal aorta and its major branches are well defined by MR, false channels within aortic dissections can be separated from the flowing channel without administration of contrast material. The use of pre-saturation pulses improve evaluation of thrombus vs slow flowing blood. Lymph nodes are readily separated from vascular structures because of the difference in signal. Non-malignant retroperitoneal fibrosis remains low in signal intensity on both T1 and T2-weighted images while malignant retroperitoneal fibrosis signal intensity is less predictable.

The MRI appearance of adrenal masses remains a challenge. Myelolipomas, simple cysts and hyperfunctioning medullary tumors have specific MR characteristics. The ability for MR imaging to differentiate non-hyperfunctioning adenomas from malignant tumor using the tumor/liver and tumor/fat signal intensity ratio has been shown to be imperfect with 20-30% of these adrenal lesions remaining indeterminate. Intravenous gadolinium perfusion of the adrenal mass has decreased this percentage to 9%.

The use of MR imaging in the diagnosis of renal masses has improved with the use of motion suppression techniques, TR/long TE sequences and the use of gadolinium

contrast agents. These improvements have permitted detection of smaller intra-renal masses and more accurate evaluation of the vascularity of these masses. MRI has been particularly useful in staging renal cell carcinoma because of the precise delineation of the renal vein and inferior vena cava. MR staging of renal cell carcinoma is especially accurate for stage IIIA-C (lymph nodes and/or vein involvement). Since slowly in-flowing blood can simulate a thrombus, pre-saturation pulses proximal to the imaging plane provide more accurate evaluation.

As the imaging speed increases, applications of MR in the kidney, adrenal and retroperitoneum are likely to expand further. MR angiography also promises to be more widely used. Breath hold images decrease the image degradation from involuntary motion flowing blood and bowel peristalsis. Dynamic scanning with gadolinium can be used to evaluate renal function despite the presence of dilatation. By varying the inversion time of the preparatory pulse in rapid imaaing, specific tissues can be nulled providing important diagnostic information.

Sunday Morning ▪ Plaza Ballroom
Educational Program ▪ EP019-EP021

Body MR Diagnostics II

10:30 AM-12:00 PM
Moderator: R J Herfkens, MD

EP019 ▪ 10:30 AM

MR of the Pelvis

Herbert Y Kressel, MD
University of Pennsylvania Hospital
Department of Radiology

The high intrinsic contrast of magnetic resonance imaging, and the ability to image in a variety of planes have resulted in a number of significant MR applications in the pelvis. Successful application of magnetic resonance techniques in the pelvis requires an understanding of the appropriate technical issues, pelvic anatomy, and the signal intensity patterns which are commonly observed in the normal and abnormal states. A number of technical advances have impacted the evaluation of the pelvis with MRI. These include multicoils, endorectal surface coils, fast spin echo pulse sequences, and gadolinium-DTPA.

Improving the signal-to-noise in pelvic examinations may be achieved through the use of surface coils, multicoils, and intracavitary coils. With multcoil technology, the signals from a number of surface coils may be combined so that signal-to-noise ratios comparable to that of surface coils may be obtained over larger fields of view. With endorectal coils, high resolution images obtained with fields-of-view as small as 8 cm can be achieved. This is particularly useful in staging prostate carcinoma, cervical carcinoma, and rectal carcinoma.

Fast spin echo techniques (RARE) are pulse sequences which allow obtaining true T2 weighted spin echo data in a fraction of the time previously required. In addition to providing excellent T2 contrast, these technques frequently demonstrate edge enhancement, and provide increased conspicuity for borders of pelvic organs. The combination of fast spin echo imaging and multicoils, allows improved resolution of normal structures in the pelvis.

In the male pelvis, MR is primarily used as a staging tool for prostate carcinoma. The zonal architecture of the prostate can be readily recognized on the T2 weighted sequences. Carcinoma which generally arises in the peripheral zone is of low signal intensity. Tumor extension beyond the capsule, into the neurovascular bundle, and seminal vesicles may be readily observed. In addition, changes of benign prostatic hyperplasia, which may vary in signal intensity can be recognized in the transition zone. Presently, MR appears to be the most accurate method of staging prostate carcinoma. In a national collaborative study comparing body coil MR and endorectal ultrasound for staging, MR was 70% accurate, whereas transrectal sonography achieved an accuracy approaching 60%. Results with the endorectal coil have been promising and demonstrate a 15% or more improvement in staging accuracy.

In the female pelvis, T2 weighted images appear to be most useful in the evaluation of the cervix, uterus, and adnexa. On T2 weighted images, the endometrial stripe, junctional zone, and peripheral myometrium may be observed. The normal ovaries can be identified in 90% of the cases by virtue of the presence of discrete ovarian follicles. Two major areas of MR application are in the evaluation of infertility, and in gynecologic oncology. MR is a useful adjunct in the evaluation of infertility. This includes congenital uterin anomalies, leiomyomas, adenomyosis, endometriosis, and other adnexal masses which may be associated with infertility. MR is also a major tool in tumor staging in the female pelvis. MR is particularly useful in evaluating cervical carcinoma, with accuracy rates approaching 90% being commonly reported. The presence of an intact, low signal, cervical stromal border to a lesion of cervical carcinoma is the most reliable sign of lack of paracervical spread. MR is also useful in assessing the depth of invasion of uterine carcinoma. Gadolinium-DTPA appears to be a useful adjunct in this regard. MR has also been reported to be of value in monitoring response to therapy and in distinguishing post treatment fibrosis from recurrent tumor . In regions of mature scar, the signal is low intensity on T2 weighted images. Recurrent carcinoma demonstrates increased signal on T2 weighted images, thus, enabling its differentiation from fibrosis.

MR is currently a major diagnostic tool in the pelvis. It is likely that as technical capabilities expand over the next several years, the range of MR applications will continue to grow.

EP020 ▪ 11:00 AM

Magnetic Resonance Imaging of the Pediatric Body

Rosalind B. Dietrich MD
University of California
Irvine Medical Center
Department of Radiological Sciences

Sedation and Imaging Techniques.

—Infants should be NPO for 2-4 hours prior to scanning.
—Older children requiring sedation should be NPO from midnight.

Children less than 2 years
—Chloral Hydrate 75m.g./k.g. (50% repeat dose at 30 mins. if needed)

Children over 2 years
Either —Thiopental 25m.g./k.g. P.R.
or —Nembutol 2.5-5m.g./K.g. I.V.
(slow titration)

Congential Anomalies.

—predominantly use thin-slice multiplanar T1-W images.
—supplemental T2-W images for evaluation of uterine anatomy or detection of ectopic testes.
—inventive use of surface coils may be necessary.

Mass Lesions.

Role of MRI is to:
—detect mass and demonstrate its organ of origin.
—aid in characterizing the mass.
—define its extent.
—evaluate vascular patency.
—demonstrate metastic lesions.

—Most cases need multiplanar T1W and T2W spin-echo pulse sequences.
—GRE and MR angiography needed for assessment of vascular patency.

Role of Gadolinium-chelates:
—better define extent of mass in relation to adjacent structures.
—increase confidence of spin-echo findings.
—help characterize mass e.g. differentiation of hemangioendotheliomas from other liver masses.

EP021 ▪ 11:30 AM

Cardiac & Thoracic Images

Robert J Herfkens, MD
Stanford University School of Medicine
Department of Diagnostic Radiology and Nuclear Medicine

The applications of magnetic resonance imaging to the cardiovascular system at one time was thought to be extremely difficult or impossible due to the motion sensitivity of magnetic resonance imaging techniques. This in fact has proven to be quite untrue. In fact, the motion sensitivity has been of great advantage in the application of MRI techniques for cardiovascular evaluation. By coordinating the acquisition to both respiratory and cardiac motion, high resolution images of cardiovascular structures can be obtained. Recent advances in fast imaging have improved the temporal resolution allowing the application of methods to dynamic imaging of cardiac of cardiac and vascular structures, providing important precise functional data about ventricular volumes, stroke volume ejection fraction and regional myocardial function. The application to routine imaging of the heart and great vessels has opened new vistas for improved sensitivity and specificity in diagnosis of complex disease. MRI has become the method of choice in a number of cardiovascular pathologies including dissecting aortic aneurysms, evaluation of great vessels and congenital heart disease, and recently MR angiography. MRI has been applied to the investigation of cardiac structure and function including ventricular volumes, motion and associated relaxation time changes with acute infarction. The development of velocity sensitive techniques has provided new methods to track individual portions of the myocardium providing unique data on myocardial motion. The combination of the tissue specificity of MRI with the improved temporal resolution associated with new fast imaging techniques have provided a unique tool in the evaluation of cardiac diseases.

Sunday Afternoon ▪ Plaza Ballroom
Educational Program ▪ EP022-EP024

Shoulder MR Imaging

1:30 PM-3:00 PM
Moderator: J B Kneeland, MD

EP022 ▪ 1:30 PM

MRI of the Shoulder: A Surgeon's Perspective

Matthew S Shapiro, MD
UCLA Medical Center
Department of Orthopedic Surgery

The role of MR imaging for assessing common shoulder problems will be discussed, particularly with respect to how these images help surgeons make clinical decisions. Shoulder problems that will be addressed include impingement syndrome, rotator cuff tears, and anterior and multidirectional instability. Pertinent anatomy and biomechanics will be reviewed, along with classification and staging systems for instability and impingement. Specific cases and pathologic anatomy relevant to these issues will be demonstrated .

EP023 ▪ 2:00 PM

SMRI: 1993
Shoulder Instability

Mahvash Rafii, MD
New York University Medical Center
Department of Radiology

Advances in cross-sectional imaging in the past decade resulted in marked improvement in visualization of the glenohumeral joint. CT-arthrography thoroughly defined the capsulolabral anatomy and displayed the various pathologic changes in detail. Despite the earlier skepticism, and with more recent advances in software and image quality, high resolution MR imaging also appears to be highly accurate in the diagnosis of glenohumeral instability by detecting tears of the glenoid labrum, abnormalities of the joint capsule, and alterations of the osseous glenoid margin and the humeral head.

Several factors should be considered in imaging of the glenohumeral joint. These include: 1) Neutral rotation of the arm. 2) Small FOV (160-140mm). 3) Thin slices (3-4mm). 4) Appropriate pulse sequence. Morphological abnormalities of the glenoid labrum are best depicted by long TR-short TE/SE sequences while the abnormal signal intensity observed on T2weighted sequences add to the specificity of findings on the intermediate sequences. The GRE or MPGR sequences should be used with caution because of a considerably higher signal intensity of the labrum degenerative change and tissue intervals and low signal intensity of the bone marrow. The most common finding in glenohumeral instability lesion is a glenoid labrum lesion which could be in the form of a substance tear seen as a high signal band-, detachment from the glenoid margin also manifested by high signal intensity and attenuation or focal absence of the labral substance. Accurate detection of labrum lesions is facilitated by familiarity with the normal capsular anatomy

and in particular knowledge of the variable features sf the glenohumeral ligaments. Alterations of the capsule such as detachment and stripping from the scapula are well visualized by MR imaging while redundancy of the capsule may not be accurately determined without the presence of joint effusion. MRI is also highly accurate in depiction of abnormalities of the osseous glenoid margin and compression fractures of the humeral head.

EP024 ▪ 2:30 PM

Magnetic Resonance Imaging of the Shoulder: Rotator Cuff Disease

J Bruce Kneeland, MD
Hospital of the University of Pennsylvania
Department of Radiology

Disease of the rotator cuff ranges from mild inflammation and degeneration to frank tear. Except for the relatively infrequent cases of acute traumatic tears, rotator cuff disease is believed to arise from impingement on the cuff by bony protrusions from the undersurface of the acromion or clavicle.

Tears of the cuff are seen as focal areas of increased signal on T2-weighted images[l]. Full-thickness tears occupy the entire thickness of the cuff whereas partial thickness tears only a portion of that thickness. In our experience, the vast majority of full-thickness tears and most of the partial thickness tears have a signal that is comparable to that of fluid on the T2 weighted images making their diagnosis relatively straightforward [2, 3]. In some cases, however, the focus of increased signal is only slightly brighter than the remainder of the cuff. In these cases it can be difficult or impossible to distinguish between a tear an a focal area of degeneration or inflammmation [4] (see below).

More diffuse foci of increased signal but with signal intensity much less than that of fluid on T2 weighted images represent either degeneration or inflammation [5]. As noted above, however, the distinction between tears and small foci of degeneration/inflammation can be difficult if not impossible to make with confidence.

The presence of one or more foci of increased signal within the cuff that are most apparent on the spin density weighted images (long TR/short TE) and difficult to visualize on the T2 weighted images has been noted in asymptomatic subjects by several investigators. Although the origin of these foci is uncertain, they should not be interpreted as representing clinically significant disease of the cuff.

In addition to detecting the presence of abnormalities of the cuff, MRI can reliably detect the presence of causes of bony impingement on the cuff including spurs on the anterior, inferior surface of the acromion and clavicle, anterior hooking to the acromion, and downward anterior and lateral tilt to the acromion, although there is disagreement among the orthopedic surgeons concerning the clinical significance of this anatomic finding. One potential pitfall that should be borne in mind is the fact that the insertion of the deltoid tendon on the acromion can mimick a spur [6]. The presence of marrow within the protrusion confirms that the structure represents a spur. The absence of marrow suggests that it could represent either tendon or spur, although according to one investigator this fact strongly favors tendon.

Several investigators have proposed the use of intra-articular Gd-DTPA solution for the evaluation of rotator cuff tears [7]. Most radiologists feel that in view of the already good accuracy of the unenhanced MRI study and the logistical problems of having to perform the injection under fluoroscopic guidance, that the intra-articular injection of Gd-DTPA should not be performed routinely.

References

1. Kneeland JB, Middleton WD, Carrera GF et al. MR imaging of the shoulder: diagnosis of rotator cuff tears. AJR 1987;149:333-337.
2. Zlatkin MB, Iannotti JP, Roberts MC et al. Rotator cuff tears: diagnostic performance of MR imaging. Radiology 1989; 172:223-229.
3. Burk DL, Karasick D, Kurtz AB, et al. Rotator cuff tears: prospective comparison of MR imaging with arthrography, sonography, and surgery. AJR 1989;153:87-92.
4. Rafii M, Firooznia H, Sherman O, et al. Rotator cuff lesions: signal patterns at MR imaging. Radiology 1990;177:817-823.
5. Kieft GJ, Bloem JL, Rozing PM, et al. Rotator cuff impingement syndrome: MR imaging. Radiology 1988;166:211-214.
6. Kaplan PA, Bryans KC, Davick JP, et al. MR imaging of the normal shoulder: variants and pitfalls. Radiology 1992;184:519-524.

Sunday Afternoon ▪ Plaza Ballroom
Education Program ▪ EP025-EP027

Other Musculoskeletal MR Diagnostics

3:30 PM-5:00 PM
Moderator: L L Seeger, MD

EP025 3:30 PM

MRI of the Knee: Meniscal and Cruciate Disorders

Leanne L Seeger, MD
UCLA Medical Center
Department of Radiology

Examination of the knee for internal derangement remains one of the most common indications for musculoskeletal MRI. Although many different imaging strategies and techniques have been proposed over the past several years, spin echo sagittal and coronal scans remain the mainstay for detecting pathology of the menisci and cruciate ligaments.

Anticipated and implemented cut-backs in third party funding for imaging studies mandate that we assess the true indications for MRI examinations, and carefully choose the patients who will benefit from this expensive test. This lecture will emphasize the role of MRI in the care of the patient with suspected internal derangement and stress potential pitfalls in image interpretation. False positive MR scans for meniscal pathology may, for example, be found if a tear has spontaneously healed or has been repaired. False negative scans may be seen with radial tears or tears at the extreme periphery or meniscocapsular junction if they are nondisplaced. Equivocal scans are often associated with acute trauma and meniscal contusion or in the severely degenerated meniscus. Cruciate ligament evaluation may also be confusing. Evaluation must include not only the appearance of the ligament, but also its course and insertions. MRI has not been shown to be sensitive for detection of partial tears of the cruciate ligaments; a partial tear may appear normal or may mimic complete disruption. The

appearance probably reflects of the percent of ligament which is torn.

EP026 ▪ 4:00 PM

Knee: None Meniscal Pathology

John V. Crues, III, MD
Cottage Community MR Center
Medical Imaging Group

The accuracy of MRI in the evaluation of meniscal pathology has been well documented. The most important diagnostic roles for MRI of the knee may well be a result of its exquisite ability to evaluate other pathology in and around the knee. The most common clinical mimic of meniscal tears and possibility the most common cause of post-traumatic knee pain are x-ray occult bony injuries. These injuries were not well recognized before the advent of MRI and are poorly detected by x-ray and surgical techniques. Many patients with post-traumatic knee pain and bony injuries may be best treated non-operatively. Ligament tears are also frequently detected after trauma and MRI is an accurate technique in detecting and characterizing these injuries. Musculoskeletal masses are common about the knee. Fortunately, most are benign and can be well characterized by MRI. MRI is less accurate in evaluating articular cartilage disease, but new techniques are being developed which may significantly improve our ability to characterize and treat articular cartilage disease. MRI of the knee's primary role is the evaluation of post-traumatic knee pain where it has been shown to be highly efficacious and cost-effective.

EP027 ▪ 4:30 PM

MRI of Soft Tissue Disorders of the Foot and Ankle

Roger M Kerr, MD
Cedars Sinai Medical Center

A variety of soft tissue processes affect the foot and ankle. These lesions usually present relatively early in their course as they may be readily palpated and, with weightbearing, may produce symptoms due to impingement upon tendons or nerves. Deep lesions may be associated with vague or poorly localized signs and symptoms and clinical diagnosis may be difficult. MRI is useful in determining the presence and extent of such lesions and in many instances may allow accurate diagnosis based on the location, signal characteristics and morphology of a lesion.

Tumors and Tumor-like lesions

The most common lesions in this category are soft tissue ganglion, plantar fibromatosis, epidermal inclusion cyst, lipoma, hemangioma, neurogenic tumors and pigmented villonodular synovitis. The most common malignant soft tissue lesion in the foot and ankle is synovial sarcoma. Many of these lesions may be accurately diagnosed by their appearance on MRI, however, confident differentiation of a benign from a malignant process is not always possible. The MR imaging features of these and other mass lesions will be discussed.

Entrapment Neuropathies

Entrapment Neuropathies result from processes that subject a nerve to increased pressure or tension. Etiologies include mass lesions, inflammation, trauma, postural deformity, accessory or hypertrophied muscle and degenerative disease. Signs and symptoms may be subtle, intermittent or poorly localized and may require physical exertion in order to be elicited. Electromyography and nerve conduction studies are not always diagnostic. MRI may be very useful in diagnosing these disorders. The anatomic and imaging features of interdigital (Morton's) neuroma and tarsal tunnel syndrome will be reviewed. Other entrapment neuropathies will also be demonstrated.

Plantar fasciitis / Heel pain syndrome

The plantar fascia is a multilayered fibrous aponeurosis that extends from the medial calcaneal tuberosity to the proximal phalanges. Repetitive trauma incites a local inflammatory reaction that produces microtears and may rarely progress to complete rupture. This process usually begins at the origin of the plantar fascia (heel pain syndrome) and extends to involve the midportion in the chronic form (plantar fasciitis). This process is often adequately assessed clinically and MRI is most useful in patients with poorly defined symptoms, in those who have failed conservative management and in assessing response to therapy. The MR imging features will be reviewed.

MON 3/29

Moderator: B J Hillman, MD, S W Young, MD

8:00 AM - 10:15 AM
New Initiatives for Funding MRI & MRS
Research at the National Cancer Institute. ..... F Shtern, MD
Pitfalls in Acquiring
MRI Equipment: Operational Experience ..... H Salmon
Evaluating New Technologies for
Policy Purposes ..... B J McNeil, MD, PhD

10:15 AM - 10:45 AM
Break ..... Grand Ballroom

10:45 AM - 12:30 PM
Financial Structuring and Dissemination
of MRI Facilities in the 90's ..... C Farnsworth
Contrast Media Research:
Implications for MRI Reimbursement ..... G L Wolf, PhD, MD

12:30 PM - 1:30 PM
Luncheon ..... Grand Ballroom

1:30 PM - 3:00 PM
Managed MRI Scan Referrals:
Economic Impact ..... J V Crues III, MD
Self-Referral and Conflict
of Interest for Diagnostic Imaging ..... B J Hillman, MD

3:00 PM - 3:45 PM
Break ..... Grand Ballroom

3:45 PM - 5:30 PM
Rate Regulation, Decreasing
Reimbursement and Strategies
for Adaption ..... M L Silbiger, MD, MBA
Competitive Strategies and
Reimbursement in MRI ..... S W Young, MD

MRI Economics Symposium

8:00 AM-10:15 AM
Moderators: B J Hillman, MD
S W Young, MD

EP028 ▪ 8:00 AM

Magnetic Resonance Spectroscopy and Magnetic Resonance Imaging: New Funding Opportunities in the National Cancer Institute (NCI)

Faina Shtern, MD, Chief,
National Cancer Institute, Diagnostic Imaging Research Branch
Wendy R Fredericks,
Program Analyst, Radiation Research Program, National Cancer Institute

The Diagnostic Imaging Research Branch (DIRB) is an extramural, research-sponsoring organization in NCI. Thus the DIRB responsibilities encompass two major tasks: 1) administration of investigator-initiated grants; 2) development of national policy in imaging science, in essence formulation of new national and international research programs.

The DIRB grant administration portfolio included total of 202 funded applications, with annual budget of about $48,349,000 in 1992. Research support in the field of Magnetic Resonance Imaging, Spectroscopy and Contrast Agents comprised about 26.9% of the branch budget ($12,981,000, or 43 grant applications (Fig. 1).

The purpose of this paper is to describe three DIRB international research programs in the area of MRS/MRI supported by NCVNIH: 1) MRS and Cancer Treatment; 2) MRS Biochemical Markers and Tumor Cell Biology; and 3) Quantitation of Tumor Response to Treatment: a 3D Approach.

[1] MRS and Cancer Treatment

The goal of this program is define the clinical role of MRI-guided localized MRS studies in early detection and prediction of tumor response to treatment in centrally coordinated, multi-institutional clinical studiesl. Specific research goals include but are not limited to the detection and prediction of immediate therapeutic response, prediction of final outcome, evaluation of the direct effect of drugs and differentiation of viable tumor from treatment-induced necrosis, edema, scar. Important features of the proposed studies will be the development of a national database for in vivo metabolic characterization of human tumors and the development of standards for the field of clinical MRS.

[2] MRS Biochemical Markers And Tumor Cell Biology

The major theme of this program is to improve understanding of fundamental tumor cell biology underpinning MRS phenomena. This DIRB program in basic MRS will address such fundamental issues in cancer cell biology as relationship between MRS markers and cell membrane metabolism, tumor physiology, genetic markers, growth receptors and drug pharmacokinetics.

[3] Quantitation of Tumor Response to Treatment: a Three-Dimensional Approach

The goal of this program, is to develop, optimize and test 3D imaging-based volumetric analysis of therapeutic response assessment. The motivation for this research stems from the current need to bring objective, automated math analysis of therapeutic response to medical oncologic practice. While the program goals address the critical issues in clinical oncology, the scientific focus of the program is on the advancement of two fundamental, generic issues in computer science: image segmentation and multimodality image registration.

1. Shtern F. NMR in Biomedicine 1992; 5: 325–328
2. Negendank W, Brown T, Evelhoch J, Griffiths J, Margulis A, Morrisett J, Ross B, Shtern F. Radiology 1992; 185:875–883
3. Shtern F, Fredericks WR. Proceedings Book, SCAR 1992: 87–91

EP029 ▪ 8:45 AM

Pitfalls of Acquiring MRI Equipment: Operational Experience

Howard Salmon
Vice President
Medical Imaging Centers of America, Inc.

With Bill Clinton in the White House, the prospects for comprehensive health care reform appear to be more likely.

That prospect coupled with already plummeting reimbursement and sky rocketing competition makes acquisition or replacement of an MRI a potentially perilous adventure.

And yet, some hospitals and clinics pay more attention to planning the annual picnic than to planning for this significant capital purchase.

The challenge, in light of likely reform, will be to provide high clinical quality, delivered in an accessible, patient sensitive manner at lower cost.

MICA has purchased over 70 MRI's in recent years. Through the acquisition decision process and subsequent operational experience, it has compiled a list of pitfalls you can avoid.

Mr. Salmon will review most of the common pitfalls,and a few of the not-so-common relating to:

- Sticker Price
- Financing
- Options and Upgrades
- Service and Maintenance
- Siting
- Field Strength
- Staffing
- Manufacturer
- Market Position

He will give examples and illustrations from multiple sites and situations.

With proper planning, common sense, and tough-minded-decision-making,you will be better prepared to make this acquisition decision in light of Clinton-style reform.

EP 030 ▪ 9:30 AM

Evaluating New Technologies for Policy Purposes

Barbara J McNeil, MD, PhD
Harvard Medical School

Material unavailable at the time of publication.

Monday Morning ▪ California Room
Educational Program ▪ EP031-EP032

MRI Economics Symposium
10:45 AM-12:30 PM
Moderators: B J Hillman, MD
S W Young, MD

EP031 ▪ 10:45 AM

"Financial Structuring and Dissemination of MRI's in the 90's" Presented by

Cherrill Farnsworth
President and CEO TME, Inc.

I. Early 90's
   A. Stark/Safeharbors
   B. Manufacturers Disarray
   C. Equipment Fallout
   D. New Capabilities
   E. Physician Partnershs and Self-Referral Prevail
   F. Mobile Companie Weaken
   G. Equipment Sales Slowing Down
   H. First Large Defaults and Non-Renewals of Equipment Leases
II. 1993
   A. Physician Partnerships Become Unacceptable
   B. Renaissance of CON
   C. Equipment Sales Stalling Out
   D. Physician Partnerships Being Purchased
   E. Very Expensive Equipment Ugrades
   F. Little New Capital Formation
      1. Fear of Healthcare Reform in Debt and Equity Markets
      2. Over Capacity
      3. Historical Defaults on Equipment Debt
      4. Disappointing Returns on Equity
III. 1993
   A. More Patients with Insurance at Lower Prices Per Scan
   B. Begin Selling Quality and Lower Costs to Educated Consumers—Insurance Companies
   C. Expensive Upgrades Will be Necessary to Survive
   D. Two to Three Years of Angst
      1. Used Equipment Available Everywhere
      2. Equipment Obsolesce by Manufacturers
      3. Mobile Companies Desperate to Place Overcapacity at Any Price
      4. Leasing Companies Drop Out
   E. Hospitals and Universities Will Join Local and Regional Networks
   F. Sole Radiology Practice Will Go Away
   G. Hospitals and Universities Will Begin Outsourcing This Service
      1. Cost Effective
      2. Radiologists Networked for Second Opinions, Depth in Practice and Regional Coverage
      3. Debt Off of Balance Sheets and Income Statements
      4. Bring Down Breakevens
IV. End of 90's—A Vastly Different Imaging Marketplace
   A. Local and Regional Networks with Hospitals, Universities, and Imaging Service Companies Working Together
   B. Only High Quality Equipment
   C. Continuing Pressure on Costs
   D. Judged on Proven Outcomes Analysis
   E. Subject to Strong Practice and Utilization Review Designed and Required by Insurance Companies

EP032 ▪ 11:30 AM

Contrast Media Research: Implications for MRI Reimbursement.

Gerald L Wolf, PhD, MD
MGH-NMR
Center for Imaging and Pharmaceutical Research

Agencies responsible for establishing reimbursement policy for health care technologies have become increasingly active. Some agencies have published policies which suggest that beneficial impact upon outcomes and cost-effectiveness are a necessary prerequisites to reimbursement. Indeed, new studies can have the effect of rescinding reimbursement for common diagnostic procedures. Our profession has not learned how to efficiently perform the studies to assure fair reimbursement for the expensive agents we use in our practice.

Monday Afternoon ▪ California Room
Educational Program ▪ EP033-EP034

MRI Economics Symposium
1:30 PM-3:00 PM
Moderators: B J Hillman, MD
S W Young, MD

EP033 ▪ 1:30 PM

Managed MRI Scan Referrals: Economic Impact

John V Crues, III, MD
Cottage Community MR Center
Medical Imaging Group

Material unavailable at the time of publication.

EP034 ▪ 2:15 PM

Conflict of Interest and Self-Referral for Diagnostic Imaging

Bruce J Hillman, MD
University of Virginia
Health Science Center
Department of Radiology

Concerns over the rate of increase in physician-related health care expenditures have reached near-crisis proportions. Analyses have targeted increasing "intensity" of care - physicians providing more and more expensive services per patient - as one of the primary reasons for increasing health care costs. Recent studies indicate that one aspect of why this may be the case is that physicians are adopting new services and technologies to which they can refer their patients that previously were predominantly the purview of other specialists. Diagnostic imaging has been a major focus for this activity, which has been dubbed "self-referral".

Public concerns about self-referral focus on professional ethics, quality of care, and cost. It is a symptom of the times that arguments over self-referral commonly are couched in the context of ethics and imaging quality; however, what is really promulgating interest in this issue are payors' and regulators' concerns about expenditures. Self-referral of diagnostic imaging takes place in two types

of settings: private offices and free-standing centers. For reasons of political expediency, the latter of these settings has received most of the attention with regard to legislative and reimbursement reform. However, self-referral in office practice is by far the more common situation, is invested with the same conflicts of interest as with self-referral in free-standing centers, and doubtlessly accounts for most of the greater expenditures research has shown to be associated with self-referral.

This presentation will probe the nature of physician conflict of interest, evaluate to what extent this conflict of interest is inextricably tied to fee-for-service reimbursement, detail the available research indicating the deleterious effects of self-referral, and describe legislative and reimbursement policy options to address the problem.

Monday Afternoon ▪ California Room
Educational Program ▪ EP035-EP036

MRI Economics Symposium

3:45 PM-5:30 PM
Moderators: B J Hillman, MD
S W Young, MD

EP035 ▪ 3:45 PM

Rate Regulation
Decreasing Reimbursement and Strategies for Adaption

Martin L Silbiger, MD, MBA
University of South Florida
Department of Radiology

In order to establish a reasonable long range plan for the development and clinical delivery of high-quality, fairly-priced imaging products, one must understand the current fiscal practice environment we live in, as well as the forces we soon will be facing nationally.

First, let us consider magnetic resonance imaging costs. Financial pro formas indicate operational costs. Included in these are the costs of equipment, financing, site preparation, depreciation, upgrading to maintain quality and currency, maintenance, personnel, overhead, supplies and bad debt. Most of the costs are fixed. In 1993, it is clear that reimbursement is relatively low and will not improve over the next decade. Factors that will allow continuing progress in magnetic resonance imaging, in a financially stable environment, will be the expanding applications of magnetic resonance imaging coupled with increasing throughput, available with new hardware and software development. Legislation limiting permissible charges for magnetic resonance procedures will work against growth in this area. An ability to understand new pressures on the industry may help us formulate a plan for growth, as well as survival.

An inherent prejudice against proliferation of costly technology in medicine is quite understandable. If a new technology is developed it will add to medical cost unless a more expensive technology is replaced. If a new technology enhances diagnostic or therapeutic abilities, what is it worth? To date, few limitations have been placed on technology, but we are facing fiscal limitations that will be mandated by Congress very soon. These, coupled with the development of clinical practice guidelines, will have a strong impact on how and how far we can go diagnostically with our patient population. The struggle will be between the real and the statistical patient. Outcomes research will certainly affect us, but so will the inherent desire to learn more about disease. Diagnostic and therapeutic algorithms will be matched with financial algorithms to determine treatment efficacy. Rationing of modern health care will be a necessary result of the failure to address the social issues of what to treat and what not to. The Oregon Medicaid fiasco is a classic example. The effort to limit those diseases Medicaid would pay for was prohibited by the Federal Government because this would officially condone rationing of health care, as if it did not already exist. Reality is a terrible thing to face, particularly for politicians.

Perhaps a more critical analysis of rising health care costs is the report of the Congressional Budget Office to the House Committee on Ways and Means. This study of the economic implications of rising health care costs presented in October, 1992, will clearly influence National health care in the coming decade. The conclusions of this study will not please many of us. Perhaps the last paragraph summarizes the problem we all face best.

But reforming the current health care system to achieve better cost control would adversely affect some of the desirable aspects of the current system. In particular, health care reform could mean less spending on research and development, longer waiting times for access to new tedhnologies, and limitations on existing choices of providers, health insurance coverage, and treatment alternatives. Whether these trade-offs are desirable depends on the priority that the nation places on controlling costs rather than maintaining the other characteristics of the health care system.

Time to roll up our sleeves and get busy.

EP036 ▪ 4:30 PM

Competitive Strategies in MRI

Stuart W Young, MD
Stanford University School of Medicine
Department of Radiology

The clinical application of MRI are continuing to expand rapidly. Advances in pulsing sequences, coil technology and the use of variable field strengths in contrast media are increasing the option available to clinicians for managing their patients with this exciting new technology. New fast scan pulse sequences have shown promising results and in conjunction with intravenous contrast media may well be modality of choice for screening patients for abnormalities in the brain and other organs. At the same time, the benefits of MRI are colliding directly with the efforts of cost containment and at a cost of between U.S. $.75M and $2M per scanner regulatory agencies throughout the world are attempting to control the diffusion and application of this expensive technology. For the clinician, however, it is progressively more important to understand both the economics and principles of MRI in order to be able to interpret adequately, and use effectively this, exciting new technology.

Acquiring the appropriate MRI system has become more complex during the last five years. In 1987, with an installed base of 1,304 MR scanners, 58% were high

field (HF) units. Although the installed base will have increased to over 3,700 MRI scanners, in 1991, only 23% of MRI unit sales (approximately 800 scanners) will be high field systems with 45% operating at mid field (MF) and 32% at ultra low field (ULF). The MRI acquisition question has become more complex because of the increasing number of MR scanners available, rapid developments in instrumentation, applications of instrumentation, cost containment efforts, and competitive factors.

The fact that the signal to noise ratio (SNR) increases approximately linearly with field strength is generally accepted at this point. High field systems are thus the clear winners when signal strength is the main objective of the clinical imaging center. Patient throughput can also potentially be traded off against the higher signal to noise of high field systems in that fewer excitations are necessary to achieve images with a diagnostic quality. Patient throughput is recognized by nearly everyone as a critical success factor, however, the types of patients being scanned, system reliability and availability of replacement parts, size of the acquisition buffer automated protocols and the systems input buffer and the ability to perform multiple tasks (filming, scanning, archiving, etc.) simultaneously, in fact, impact patient throughput to a greater extent than SNR.

In an ever more competitive imaging environment, the interrelationship between instrumentation, MRI application, and cost factors has become increasingly important. The acquisition price is, of course, important but, product cycle costs are also important and mid and low field systems are generally estimated to cost only 30% to 40% of high field systems over a five-year time frame. Siting, shielding, manufacturer's reputation and stability, local referral patterns and the types of systems operated by compctitors, pulsing sequence and RF coil flexibility, system reliability and local service availability, upgrade ability, patient comfort, and architecture of the system represent a complex fabric of interrelated factors which vary in importance from practice to practice.

There are three components with respect to the charges for MRI procedures. A technical component relates to the imaging centers' cost of equipment, labor, and overhead. The professional fee covers the radiologists work of interpretation and there is a fee associated with the use of contrast media. In 1991, approximately 28% of the procedures performed in the United States, utilized MRI contrast media (1). In a study conducted by the Society of Magnetic Resonance Imaging (2) collections for these three components were as follows: technical fee: $650; professional fee: $225; contrast media: $210. The range for each one of these categories is, however, quite large and these figures are relatively close to those which have been reported by others (3).

Professional and technical fees are associated with each scan performed, so the collection for performing 6.4M scans is as follows: 6.4M x ($653 + $225) = $5,619M. In addition, approximately 28% of these scans will receive contrast media as follows: 6.3M scans x 28% x $210 per contrast media dose = $370.44M. This gives a total expense for MRI scanning in the United States in 1991 as $5,989M .

In conclusion, any consideration of MRI today should be placed in a context of the overall imaging and health care environment with respect to the major imaging trends, a potential strategy for dealing with these changes, and tactics for dealing with an increasingly uncertain environment.

Scientific Program Works in Progress Proffered Papers

MON 3/29

10:45 AM - 12:30 PM

Papers 101-108
Head and Neck I
Franciscan Room B

Moderators:
A N Hasso, MD
W R K Smoker, MD

101 **10:45 AM**
102 **10:57 AM**
103 **11:09 AM**
104 **11:21 AM**
105 **11:33 AM**
106 **11:45 AM**
107 **11:57 AM**
108 **12:09 PM**

Papers 109-116
Contrast Agent II: Experimental I
Franciscan Room C

Moderators:
W G Bradley, Jr, MD, PhD
D D Stark, MD

109 **10:45 AM**
110 **10:57 AM**
111 **11:09 AM**
112 **11:21 AM**
113 **11:33 AM**
114 **11:45 AM**
115 **11:57 AM**
116 **12:09 PM**

Papers 117-124
MRA: Clinical I
Plaza A

Moderators:
R A Clark, MD
P J Fritzsche, MD

117 **10:45 AM**
118 **10:57 AM**
119 **11:09 AM**
120 **11:21 AM**
121 **11:33 AM**
122 **11:45 AM**
123 **11:57 AM**
124 **12:09 PM**

Papers 125-132
Rapid Imaging Techniques I
Plaza B

Moderators:
M S Cohen, PhD
S R Thomas, PhD

125 **10:45 AM**
126 **10:57 AM**
127 **11:09 AM**
128 **11:21 AM**
129 **11:33 AM**
130 **11:45 AM**
131 **11:57 AM**
132 **12:09 PM**

Papers 133-140
Breast
Imperial Ballroom

Moderators:
R Kikinis, MD
M L Silbiger, MD

133 **10:45 AM**
134 **10:57 AM**
135 **11:09 AM**
136 **11:21 AM**
137 **11:33 AM**
138 **11:45 AM**
139 **11:57 AM**
140 **12:09 PM**

Papers 401-410
WIP 1: MRI-Clinical
Franciscan A

Moderators:
J D Rubenstein, MD
F G Shellock, PhD

401 **10:45 AM**
402 **10:55 AM**
403 **11:05 AM**
404 **11:15 AM**
405 **11:25 AM**
406 **11:35 AM**
407 **11:45 AM**
408 **11:55 AM**
409 **12:05 PM**
410 **12:15 PM**

TUE 3/30

10:30 AM - 12:15 PM

Papers 201-208
Cardiac II
California Room

Moderators:
L Eastwood, PhD
C B Higgins, MD

201 **10:30 AM**
202 **10:42 AM**
203 **10:54 AM**
204 **11:06 AM**
205 **11:18 AM**
206 **11:30 AM**
207 **11:42 AM**
208 **11:54 AM**

Papers 209-216
Abdomen
Franciscan Room B

Moderators:
D G Mitchell, MD
P Y Poon, MD

209 **10:30 AM**
210 **10:42 AM**
211 **10:54 AM**
212 **11:06 AM**
213 **11:18 AM**
214 **11:30 AM**
215 **11:42 AM**
216 **11:54 AM**

Papers 217-224
Brain
Plaza A

Moderators:
K R Maravilla, MD
A S Smith, MD

217 **10:30 AM**
218 **10:42 AM**
219 **10:54 AM**
220 **11:06 AM**
221 **11:18 AM**
222 **11:30 AM**
223 **11:42 AM**
224 **11:54 AM**

Papers 225-232
Rapid Imaging Techniques II
Plaza B

Moderators:
J Listerud, MD, PhD
S J Riederer, PhD

225 **10:30 AM**
226 **10:42 AM**
227 **10:54 AM**
228 **11:06 AM**
229 **11:18 AM**
230 **11:30 AM**
231 **11:42 AM**
232 **11:54 AM**

Papers 233-240
Contrast Agent III: Experimental II
Imperial Ballroom

Moderators:
T J Brady, MD
R L Nunnally, PhD

233 **10:30 AM**
234 **10:42 AM**
235 **10:54 AM**
236 **11:06 AM**
237 **11:18 AM**
238 **11:30 AM**
239 **11:42 AM**
240 **11:54 AM**

Papers 411-420
WIP 2: MRI-Rapid Imaging and Contrast Material
Franciscan A

Moderators:
S M Brown, MD
J F Norfray, MD

411 **10:30 AM**
412 **10:40 AM**
413 **10:50 AM**
414 **11:00 AM**
415 **11:10 AM**
416 **11:20 AM**
417 **11:30 AM**
419 **11:40 AM**
418 **11:50 AM**
420 **12:00 PM**

WED 3/31

10:30 AM - 12:15 PM

Papers 301-308
Spectroscopy II
California Room

Moderators:
G B Matson, PhD
J A Sorenson, PhD

301 **10:30 AM**
302 **10:42 AM**
303 **10:54 AM**
304 **11:06 AM**
305 **11:18 AM**
306 **11:30 AM**
307 **11:42 AM**
308 **11:54 AM**

Papers 309-316
MRI: General
Franciscan Room B

Moderators:
M R Fisher, MD
N J Pelc, ScD

309 **10:30 AM**
310 **10:42 AM**
311 **10:54 AM**
312 **11:06 AM**
313 **11:18 AM**
314 **11:30 AM**
315 **11:42 AM**
316 **11:54 AM**

Papers 317-324
Flow Velocity II
Plaza A

Moderators:
R S Hinks, PhD
S R Thomas, PhD

317 **10:30 AM**
318 **10:42 AM**
319 **10:54 AM**
320 **11:06 AM**
321 **11:18 AM**
322 **11:30 AM**
323 **11:42 AM**
324 **11:54 AM**

Papers 325-332
MRA: Clinical II
Plaza B

Moderators:
C Dumoulin, PhD
T R McCauley, MD

325 **10:30 AM**
326 **10:42 AM**
327 **10:54 AM**
328 **11:06 AM**
329 **11:18 AM**
330 **11:30 AM**
331 **11:42 AM**
332 **11:54 AM**

Papers 333-340
Contrast Agent IV: Brain and Miscellaneous
Imperial Ballroom

Moderators:
S B Peterman, MD
G K Sze, MD

333 **10:30 AM**
334 **10:42 AM**
335 **10:54 AM**
336 **11:06 AM**
337 **11:18 AM**
338 **11:30 AM**
339 **11:42 AM**
340 **11:54 AM**

Papers 421-430
WIP 3: MRI-Technical
Franciscan A

Moderators:
L P Clarke, PhD
J Illes, PhD

421 **10:30 AM**
422 **10:40 AM**
423 **10:50 AM**
424 **11:00 AM**
425 **11:10 AM**
426 **11:20 AM**
427 **11:30 AM**
428 **11:40 AM**
429 **11:50 AM**
430 **12:00 PM**

MR 1993

PROFFERED PAPERS

The 1993 Works in Progress Program will present 30 presentations, Monday, March 29 – Wednesday, March 31 during the Scientific Program morning parallel sessions. Abstracts may be found on the following pages. To plan your itinerary, refer to the preceding page for a complete listing of the morning sessions.

Seating for the scientific sessions is on a space-available basis. You are invited and encouraged to move from one meeting room to another during a time block to hear different presentations. Please, however, be sensitive to the presenter and the other attendees while implementing your itinerary.

SMRI '93 Works in Progress

Proffered Paper Abstracts

Monday Morning • Franciscan A
Papers 401–410

WIP 1: MRI–Clinical

MODERATORS: JD Rubenstein, MD
FG Shellock, PhD

401 • 10:45 AM

MR Prostate Bulge Sign: Valid Sign of Transcapsular Spread of Carcinoma

TL Krebs, JM Silverman, GA Pjura, J Ohara
Department of Radiology, Cedars-Sinai Medical Center, Los Angeles, CA

Purpose: Recent literature indicates that sonographic detection of a focal hypoechoic subcapsular bulge is an accurate indicator of transcapsular spread of carcinoma. This study was performed to determine if MR visualization of a similar tumor bulge predicts extraglandular extension of tumor.
Methods: We performed a retrospective analysis of 220 cases of prostate carcinoma imaged on a 1.5-T MR imager with an endorectal surface coil. A positive prostate bulge sign was defined as a focal contour abnormality with characteristic T2 signal hypointensity. Two radiologists, specializing in MR, independently reviewed the studies for the presence of the MR bulge sign; both were blinded as to final pathologic diagnosis.
Results: The MR prostate bulge sign was detectable in 67 cases, of which 32 had pathologic correlation. MR correctly predicted focal transcapsular spread of tumor in 26 cases for a positive predictive value of 81%.
Conclusion: Accurate preoperative prostate cancer staging is essential for proper therapeutic decision analysis. The MR prostate bulge sign, although present in a minority of patients, is a reliable predictor of extraglandular spread of tumor.

402 • 10:55 AM

MR Imaging in the Evaluation of Fecal Incontinent Patients for Indication and Planning of Corrective Surgery

LA Rosemberg, ACA Magalhaes, MA Marotti, R Galves, AEA Magalhaes
Hospital das Clinicas-FMUSP, Sao Paulo, Brazil

Purpose: Patients with anorectal malformation (ARM), Fournier syndrome (FS), and perineal trauma (PT) were evaluated with MR imaging to establish the possibility of corrective surgery to improve their perineal anatomy and fecal continence with a posterior sagittal anorectoplasty (PSARP). We studied the relationship between the anorectal canal and the pelviperineal muscles that are classified on the basis of their group function and intraoperative muscle stimulation pattern: parasagittal fiber, muscle complex, and levator groups.
Methods: MR imaging was performed with a Signa 1.5-T unit (GE, Milwaukee) in 15 patients (ARM = 12, FS = 1, and PT = 2 cases). Children were examined under sedation or anesthesia. The perineal line was demarcated with a tube filled with oil and the anorectum with a rectal tube filled with air. Coronal, sagittal, and axial T1- and T2-weighted images were obtained with a section thickness of 3–5 mm. The head coil, surface coil, and body coil were used in that order of preference. The ARM patients had been operated on before with other surgical techniques and continued to have fecal incontinence.
Results: The criteria for reoperation were a mislocated anorectal canal with preserved pelviperineal muscles and normal sacrum. Surgery was indicated in 5 patients who fulfilled these criteria (ARM = 4 and PT = 1). At surgery, the MR imaging findings were confirmed. The other patients continued with clinical management due to a deficient pelviperineal musculature and a mislocated anorectal canal in 7 cases (ARM = 7), muscle abnormalities in 2 cases (PT = 1 and FS = 1), and a sacral abnormality in 1 case (ARM).
Conclusion: With this series, we conclude that MR imaging should be used in all patients with fecal incontinence that cannot be controlled clinically, especially patients who have already undergone a surgical procedure.

403 • 11:05 AM

Three-dimensional MR Cholangiography: Single-Slab and Single-Breath-Hold Technique

K Morimoto, M Shimoi, T Shirakawa, Y Aoki, S Choi, M Mitomo, Y Miyata
Department of Radiology, Osaka National Hospital, Osaka, Japan

Purpose: To simplify the method of three-dimensional MR cholangiography, we developed a single-breath-hold technique. With our new technique, all the image data from the biliary tree can be obtained in a single slab during a single breath hold.
Methods: We have already reported the method of three-dimensional MR cholangiography using the multiple 3D slab technique (Radiology 183: 578–580 1992). It requires several repetitions of 20-second breath holding to obtain all the image data from the biliary tree. The previous TR and TE of CE-FAST, which was used for this technique, were 17 and 7 msec, respectively. In this pulse sequence, the numbers of slab partitions were limited to 8. By modifying the TR and TE to 12 and 4 msec, 16 slab partitions could be used. With this modification, two times as much data sampling area could be obtained in a single slab during a 20-second breath hold. By widening the slab thickness from 32 to 128 mm, the whole area of the biliary tree can be covered in a single slab. Also, by using 8 slab partitions with these parameters, all the image data could be obtained in only 10 seconds of breath holding. We have evaluated this technique in 10 patients with biliary and pancreatic diseases.
Results: In all patients, high image quality and the same detectability as with the previous method was obtained.

Conclusion: By reducing imaging and breath-hold time, this technique can be applied widely.

404 • 11:15 AM

"Magic Angle" Phenomena in MR Imaging of Bovine Articular Cartilage

JD Rubenstein, JK Kim, I Morava-Protzner, P Stanchev, RM Henkelman

Department of Radiology, University of Toronto, Sunnybrook Health Science Centre, Toronto, Ontario, Canada

Purpose: Previous MR studies show that normal articular cartilage has a laminated appearance. Our hypothesis for this study was that the internal collagen structure of cartilage and its orientation influence the appearance of the laminations by an anisotropic T2 effect.

Methods: T1-weighted axial MR images of cartilage from 18 bovine patellae were obtained with specimen rotation about the vertical axis of the patella in 5° increments between +75° and −130°. Signal intensity profiles of the cartilage layers were obtained at each rotation and average signal from each lamination was plotted against rotation angle to assess orientation dependence of signal from each lamina.

Results: MR imaging showed three cartilage laminae (superficial high signal, middle low signal, and deep intermediate signal) along articular surfaces facing 0° and −90° to B_0. Signal intensity of the middle lamina increased to a maximum at +55°, −55°, and −125° ("magic angles"), producing a homogeneous appearance of the cartilage. Quantitative measurements show signal intensity changes of the superficial and middle laminae with rotation angle. Failure to orient the planar surface of the cartilage perpendicular to the imaging plane also resulted in a homogeneous appearance of the cartilage due to partial-volume effects.

Conclusion: The anisotropic arrangement of the collagen fibers in cartilage, particularly where collagen orientation is radial to the articular surface, strongly influences the laminated MR appearance of articular cartilage. We conclude that orientation of the cartilage relative to B_0 is an important determinant in the MR appearance of articular cartilage.

405 • 11:25 AM

MR Imaging Evidence of Marrow Reconversion Secondary to Granulocyte Colony Stimulating Factor: Potential Pitfall in Tumor Evaluation

SP Ryan, E Weinberger, DWW Shaw, KS White, J Miser, V Nazar-Stewart

Department of Radiology, Children's Hospital and Medical Center, Seattle, WA

Purpose: Granulocyte colony stimulating factor (GCSF) is used to stimulate myeloid cell proliferation in patients undergoing chemotherapy. We hypothesize that the use of GCSF is associated with MR imaging changes consistent with reconversion from fatty to hematopoietic marrow.

Methods: Thirty-nine MR imaging examinations in 16 patients with osteogenic sarcoma (OGS) were evaluated by three blinded observers. A 5-point scale (referenced to normal fat and muscle signal intensities) was used to grade marrow signal intensity in metaphyseal and diaphyseal locations remote from tumor. Decrease in T1 signal and/or increase in STIR signal of 2 points was classified as reconversion. Rates of marrow reconversion for the GCSF and non-GCSF patients were compared by relative risk analysis.

Results: Ten of 16 patients received GCSF. The groups were otherwise similar. MR imaging evaluations were consistent between observers. Reconversion was found in 7 of 10 GCSF patients but in none of 6 in the non-GCSF group (relative risk of 4.9; 95% confidence interval, 0.8–31.5). No marrow recurrences were found at follow-up.

Conclusion: Patients undergoing chemotherapy for OGS who receive GCSF have a high likelihood of developing MR imaging changes consistent with reconversion in marrow sites remote from the primary tumor. Awareness of this finding could reduce false-positive diagnosis of marrow metastases. Proposed future work includes correlation of MR imaging findings with pathologic examination of excised specimens.

406 • 11:35 AM

MR Imaging of Silicone Breast Implants with an Inversion-Recovery Fast Spin-Echo (IR-FSE) Pulse Sequence

FG Shellock, B Rothman, RJ Brenner, S Hinks, A Sawyer

Tower Imaging, Los Angeles, CA

Purpose: MR imaging of silicone breast implants is typically performed with fat-suppressed, T2-weighted pulse sequences. Unfortunately, a fat-suppression sequence also suppresses the signal of silicone and does not provide optimum contrast between the implant and surrounding tissue. An IR-FSE pulse sequence was used to image water, peanut oil, and silicone implant phantoms. The IR-FSE provided good contrast compared with a T2-weighted, fat-suppressed sequence. Accordingly, IR-FSE was used to image patients for evaluation of suspected silicone implant leaks or ruptures.

Methods: Eleven patients (22 breasts) with bilateral silicone (n = 20) or silicone/saline implants (n = 2) were imaged with a 1.5-T MR imager (GE Medical Systems) and either dual shoulder coils or a wraparound flex coil. Images were obtained with axial IR-FSE; T1-weighted, FSE; T2-weighted, water and fat suppressed FSE; and sagittal proton density and T2-weighted FSE pulse sequences. Images were qualitatively evaluated with respect to the tissue/implant contrast and assessed for the presence of implant leaks or ruptures with previously reported criteria.

Results: Images obtained with the IR-FSE pulse sequence showed fat with an intermediate signal intensity and silicone with increased signal intensity, allowing good contrast for determination of ruptures or leaks. Sixteen breast implants had no leak or rupture, four had intracapsular ruptures, and two had extracapsular leaks.

Conclusion: The tissue contrast characteristics of the IR-FSE pulse sequence showed the best differentiation between the silicone implant and surrounding breast tissue compared with the other pulse sequences. The IR-FSE pulse sequence appears to be useful for evaluating patients with silicone breast implants.

407 • 11:45 AM

MR Imaging in Chagas Disease: Signal Intensity and Pathologic Correlation

LA Rosemberg, ACA Magalhaes, R Kalil, AEA Magalhaes, C Mady, ACP Barreto, F Pileggi

Hospital das Clinicas-FMUSP, Sao Paulo, Brazil

Purpose: We tested the hypothesis that MR imaging can help distinguish patients with myocarditis in Chagas disease (CD) heart failure from patients with heart failure due to idiopathic dilated cardiomyopathy (IDC).

Methods: Short-axis and transverse spin-echo images, electrocardiogram gated, were acquired on a Signa 1.5-T system (GE, Milwaukee) (TE = 25 msec, TR = R-R interval, section thickness = 8 mm) in 6 men with CD (age, 43 years ± 5) and compared with 6 with IDC (age, 47 years ± 7). Myocardial septal intensity was compared with that of thoracic skeletal muscle before and after bolus injection of 0.1 mmol/kg Gd-DTPA. Septal biopsies were performed within 24 hours of MR imaging in all patients.

Results: Inflammation was observed in septal biopsy specimens in all CD but in none of the IDC subjects, as assessed by the Dallas criteria. MR imaging demonstrated increased signal intensity after Gd-DTPA (1.54 ± 0.16 vs 0.87 ± 0.05 before Gd-DTPA, $P < .001$) in CD but not in noninflammatory IDC (0.93 ± 0.07 vs 0.89 ± 0.06 before Gd-DTPA, P = ns).
Conclusion: The findings of increased, heterogeneous myocardial signal intensity after gadolinium infusion in inflammatory CD suggests that MR imaging could have a potential role in the noninvasive diagnosis of myocarditis in CD.

408 • 11:55 AM

High-Resolution Coronal MR Imaging Myelography

J Silverman, FG Moser, BD Pressman, EJ Tourjé
Cedars-Sinai Medical Center, Los Angeles, CA

Purpose: MR imaging has become the primary technique used in the evaluation of degenerative disease of the lumbar spine. Despite this, the number of conventional myelograms performed continues to remain high at many institutions. This is due in part to the perception by many nonradiologists that a better assessment of the neural structures within the spinal canal can be made with conventional myelography and/or CT myelography. We have developed a high-resolution, heavily T2-weighted fast spin-echo technique that results in images that have the visual appearance of a conventional myelogram.
Methods: The imaging is performed in the coronal plane with a fast spin-echo sequence with 15 contiguous 4-mm thick sections, with a TR of 5,000 msec and effective TE of 256 msec. An echo train length of 16 is used. A data matrix of 512 × 256 provides high resolution. The acquisition time is 2 minutes 40 seconds. The images are "collapsed" and projected in the coronal plane and rotated around the longitudinal axis.
Results and Conclusion: This technique produces images highly reminiscent of conventional myelography, with accurate depiction of nerve roots, root sleeve amputations, and extradural defects. Additionally high-resolution imaging of intradural tumors and vasculature is possible. To date, over 200 patients have been studied with this technique with great success. Examples of different pathologies will be presented.

409 • 12:05 PM

Development of an MR Imaging–Compatible RF and Temperature Probe for MR-Guided Tumor Ablation

S Sinha, Y Anzai, E Behnke, J Parker, A Desalles
UCLA Medical Center, Los Angeles, CA

Purpose: To develop an MR-compatible radio-frequency (RF) ablation system, allowing transmission and temperature-sensing, which would permit MR-guided tumor ablation simultaneously with image acquisition.
Methods: A 18-gauge MR-compatible needle (E-Z-Em, Westbury, NY), was converted into the live component of a coaxial RF probe, using an electrically insulating varnish over the outer surface except for 3 mm at the tip. A Teflon-insulated copper-constantan thermocouple (Omega Engineering, Stamford, CT), was positioned inside the needle for dynamic temperature monitoring. An RF lesion generator system, (Radionics, Burlington, MA), producing a 480 kHz sine wave was used for RF irradiation of tissue. The device was tested in phantoms and an animal model with a 1.5-T clinical MR unit.
Results: The thermocouple functioned well in the magnetic field. Noise generated from the RF module was sufficiently low so that simultaneous monitoring, RF irradiation, and MR image acquisition (using FAST spin-echo techniques for monitoring of lesion size and appearance) could be performed.
Conclusion: With this technique, it is now possible to perform RF tissue ablation with thermal feedback during MR image acquisition, thus providing a more complete and real-time picture of the histopathologic changes induced therein.

410 • 12:15 PM

MR Imaging–guided Laser-induced Interstitial Thermotherapy in Cerebral Malignancies

T Kahn, F Ulrich, M Bettag, M Deimling, U Mödder
Institute of Diagnostic Radiology, University of Düsseldorf, Düsseldorf, Germany

Purpose: Laser-induced interstitial thermotherapy (LITT) by stereotaxic low-power irradiation with a 1,064 nm Nd:YAG laser is a new therapeutic approach in the treatment of brain tumors. The purpose of our study was the determination of the value of MR imaging in monitoring LITT.
Methods: We have performed LITT in 7 patients (28–73 years old; mean, 58 years) with astrocytoma (n = 5), metastasis (n = 1), and lymphoma (n = 1). The diameter of the tumors ranged from 15 to 31 mm. CT-guided biopsy followed by implantation of an applicator probe (Teflon catheter, 6 F) according to the stereotaxic coordinates was performed. The tip of the applicator probe was placed 10 mm proximal to the margin of the tumor. After replacing the coordinate ring system, the patients were transferred to the MR department and a special light guide with a directed circumferential beam characteristic (ITT light guide, MBB-Medical Technology, Ottobrunn, Germany) was introduced via the applicator to the tumor center. The position of the light guide was controlled with multiplanar reconstructions of a T1-W Turbo-FLASH sequence. During the course of laser intervention (8–20 minutes, depending on the results of the MR study, continuous waves at a power of 4 W) a 2D FLASH sequence (70/6, FA = 70°, section thickness = 3 mm, 5 sections, acquisition time 15 sec) was repeatedly used. The procedure was performed under local anesthesia and was well tolerated by all patients. Thirty-five follow-up MR studies were performed (longest follow-up period, 14 months).
Results: In all patients, a gradually increasing zone of high signal intensity (T1-W) surrounding the tip of the light guide developed during therapy (maximum diameter, 5–18 mm). This was surrounded by a low-signal-intensity rim (T1-W). On T2-W posttherapy images the signal intensities of the two zones were reversed. The posttherapy T1-W images after Gd-DTPA showed rimlike local disruption of the blood-brain barrier at the borders of the peripheral zone. Total lesion size ranged from 12 to 32 mm. Immediately after therapy, the central zone comprised 44%–56% of total lesion size. Three to 10 days after therapy the total lesion size showed no significant change. However, the size of the central lesion increased and comprised 64%–71% of total lesion size. Additional perifocal edema increased directly after therapy with a space-occupying effect in 5 patients. The follow-up studies showed a continuous reduction in lesion size and a regression of the edema.
Conclusion: The results of our study demonstrate the ability of MR imaging in monitoring LITT.
M. Deimling is an employee of Siemens.

WIP 2: MRI–Rapid Imaging and Contrast Material

MODERATORS: SM Brown, MD • JF Norfray, MD

411 • 10:30 AM

Mechanism of Liver MR Imaging Signal Enhancement with Gd-BOPTA/Dimeg

FM Cavagna, V Lorusso, F Maggioni, G Visentin, C de Haën
Bracco SpA, R&D Division, Milan, Italy

Purpose: To assess contributions of contrast agent (CA) in bile and hepatocytes to enhanced liver parenchymal signal intensity (SI) after administration of Gd-BOPTA/Dimeg.
Methods: In dogs with a cannulated bile duct and occluded cystic duct, bile fractions were collected after intravenous administration of 200 μmol/kg of 0.5 M Gd-BOPTA/Dimeg (gadobenate dimeglumine). CA concentration and SI of the fractions were determined with HPLC and with SE 200/16 images taken at 0.5 T, respectively. Transverse abdominal MR images were taken after the same dose of CA using the same imager and sequence (FOV = 16 cm^2, matrix = 256^2, section thickness = 2 mm).
Results: Gd-$BOPTA^{2-}$ concentration in the bile increased to a maximum of 20 mM at 45 to 60 min after administration, then decreased slowly and still amounted to 8 mM at 360 min. Bile fraction MR SI and in vivo hepatic bile duct SI, with similar time profiles, showed early peaks at 0–15 min. Owing to predominant T2 relaxation, SI then decayed quickly to values below those before CA administration. Relative to the parenchyma, the SI of which was persistently enhanced after CA administration, bile ducts went from being hypointense before CA administration to hyperintense 5 min after and again hypointense 13–240 min after.
Conclusion: Liver parenchymal signal enhancement is due to the high relaxivity of the agent inside hepatocytes and is little affected by its presence in bile.
F.M. Cavagna is an employee of Bracco SpA.

412 • 10:40 AM

T2 Relaxation Effect of Iron Oxide Depends on Its Spatial Distribution

A Tanimoto, BP Kreft, Y Baba, JT Chen, Y Yuasa, DD Stark
Keio University School of Medicine, Tokyo, Japan

Purpose: It has been documented that the T2 relaxation effect of superparamagnetic iron oxide (SPIO) depends on its particle size, magnetic properties, and echo time used. We investigated whether the T2 relaxation effect of SPIO depends on its spatial distribution.
Methods: To investigate the T2 relaxation effect of SPIO under different spatial distribution, phantoms of agar gel only (control) and one with added Sephadex beads, and normal control rats and rats with carbon tetrachloride-induced hepatitis, were prepared. Phantoms were doped with different concentrations of SPIO-dextran, and animals were injected with SPIO (20 μmol/kg). Relaxometry (0.47 T) was performed and light microscopic sections were obtained for phantoms and liver specimens, and MR imaging (SE 300/10, SE 2,000/45, 90) at 1.5 T was performed in phantoms and animals.
Results: Phantoms with added Sephadex beads and diseased livers showed heterogeneous distribution of SPIO, compared with controls. Relaxometry showed a decreased R2/R1 ratio of SPIO in phantoms with added Sephadex (R2/R1 = 2.5) compared with controls (3.6), and less T2 relaxation effect relative to T1 relaxation effect in diseased liver tissue than in controls. Signal-to-noise ratios of phantoms with added Sephadex and of diseased livers showed a smaller decrease on T2-weighted images and an absolute increase on T1-weighted images, compared with controls.
Conclusion: Sparsely distributed SPIO show a decreased T2 relaxation effect. Under such conditions, T1 relaxation effects of SPIO may predominate, resulting in a signal intensity increase in the liver on T1-weighted images. This finding may influence applications of SPIO for detection and quantitation of liver injury.

413 • 10:50 AM

New Extracellular, Nonionic Chelates for MR Imaging Liver Enhancement

WA Gibby, NR Puttagunta, GA Leach
Department of Radiology, Utah Valley Regional Medical Center, Provo, UT

Purpose: We sought to develop a nonionic extracellular chelate with liver affinity that would be renally eliminated.
Methods: Gd-DTPA bis-glucosamide (Gd-DTPAGluc), Gd-DTPA bis-galactosamide (Gd-DTPAGal), and Gd-DTPA bis-pyridoxamide (Gd-DTPAPyr) were synthesized. Pre- and postcontrast images of liver, kidney, and muscle were obtained with NZW rabbits in a clinical imager at 1.5 T. Competitive HPLC with fluorescent detection was used to determine relative ligand stability against EDTA and DTPA and metal ion selectivity against Cu-EDTA and Zn-EDTA. Minimum lethal doses were determined in mice for Gd-DTPAGluc and Gd-DTPA.
Results: Liver enhancement for Gd-DTPAGluc, Gd-DTPA-Gal, and Gd-DTPA were 19%, 19%, and 4.8%, respectively, at 11 minutes, and 15%, 9.4%, and −2.7%, respectively, at 54 minutes. For the same agents, the enhancement of the kidney was 69%, 45%, and 52% at 11 minutes and 32%, 33%, and 28% at 54 minutes. Muscle enhancement was variable. Gd-DTPAPyr exhibited variable liver enhancement, which slowly rose for the first 1 1/2 hours to a maximum of 15%. Relative ligand stability for Gd-DTPAGluc and Gd-DTPAGal was comparable with that of Gd-DTPA at pHs of 5.8 and 7.4. Metal selectivity on a molar ratio was three times better for Gd-DTPAGluc than for Gd-DTPA when titrated with copper or Zn-EDTA. Minimum lethal dose of Gd-DTPAGluc was 20 mM/kg in mice, compared with 4 mM/kg for Gd-DTPA.
Conclusion: Both Gd-DTPAGluc and Gd-DTPAGal exhibit a fourfold improvement in liver enhancement compared with Gd-DTPA at 11 minutes. Gd-DTPAGluc is a nonionic agent excreted by the kidneys, with low toxicity and good ligand stability. It shows promising liver enhancement while performing the other functions of an extracellular fluid agent.

414 • 11:00 AM

Positive or Negative Enhancement Properties of Superparamagnetic Nanoparticles in MR Lymphography: Differentiation Between Inflammatory and Metastatic Lymph Nodes

R Guinares, J Bittoun, F Carnot, E de Kerviler, G Frija
Department of Radiology, Hospital Boucicaut, Paris, France

Purpose: Besides their well-known T2* properties, ultrasmall superparamagnetic iron oxides (USPIO) can act as positive enhancers at low concentration with a T1-weighted sequence. This study investigates the positive and negative enhancement patterns of inflammatory and metastatic lymph nodes after different intravenous doses of USPIO with various sequences.
Methods: Inflammatory and tumorous lymph nodes were

obtained in rats and imaged in vivo at 1.5 T before and 24 hours after intravenous injection of AMI227 (Advanced Magnetics, 40–200 μmol Fe/kg). Different spin-echo and gradient-echo sequences were tested. Lymph nodes were surgically harvested and then in vitro high-resolution (HR) imaging was done in the same magnet with a prototype coil allowing a pixel size of 70 × 200 μm. HR images were correlated with histology and iron staining.
Results: Inflammatory nodes showed, in vivo and in vitro, a heterogeneous uptake for doses of 80 μmol Fe/kg or higher. Particles clustering in the macrophages of the periphery and hilum of the node always resulted in a negative enhancement with every sequence. For tumorous nodes, a dark rim was seen in the periphery for the same doses, but positive enhancement of the metastasis center was seen with T1-weighted sequences for 200 μmol Fe/kg.
Conclusion: USPIO induce a heterogeneous negative enhancement of inflammatory nodes. In tumorous nodes, particle leakage into the interstitial space of the tumor results in a positive enhancement of the center of the node with T1-weighted sequences.

415 • 11:10 AM
FSE Pelvic MR Imaging with External Helmholtz Coil Compared with Body Coil
JF Norfray
Chicago Northside MRI Center, Chicago, IL

Purpose: To determine if the external Helmholtz pelvic coil (PC) improves S/N compared with the body coil (BC) and to identify problems related to PC and FSE imaging.
Methods: Twenty-nine patients (16 women, 13 men) were imaged. Abnormalities included gynecologic (13), genitourinary (12) (including 10 carcinomas of the prostate), gastrointestinal (2), obstetric (1), bone (1). Weight of patients ranged from 93 to 220 pounds, with 5 patients weighing more than 200 pounds. FSE was performed in the axial plane with both coils. Coronal T1-, axial T1-, and sagittal T2-weighted images were obtained only with PC, keeping the total imaging time to 30 minutes. FSE technique: TR = 4,000, TE = 17/102, ETL = 8. FOV = 20, matrix = 256, fat saturation.
Results: (1) PC improved S/N in all patients compared with BC. (2) A spinal bone lesion in S-1 was poorly seen with PC because of signal dropoff; all other PC studies had adequate coverage. (3) Problems identified with the pelvic coil included (*a*) centering—coils placed too far from or too close to the perineum; (*b*) decoupling—touching of the anterior coil to the lower abdomen caused decoupling in 3 patients with abdominal breathing; and (*c*) hot spot—proximity of anterior coil to abdominal wall caused phase error in 15 patients on the sagittal view. (4) Problems due to FSE included blurring of the sagittal proton-density image (TE = 17) in 15 patients.
Conclusion: (1) External Helmholtz pelvic coil improves S/N compared with BC technique. (2) New coil design eliminates the decoupling of the coils. (3) Phase artifacts on sagittal images can be suppressed by changing the phase direction and using superior saturation. (4) Blurring of the proton image in FSE can be suppressed by decreasing the ETL to 4.

416 • 11:20 AM
New Coil Design for Small-FOV Pelvic Imaging
S Jarso, RH Patt, SH Ascher
Department of Radiology, Georgetown University Hospital, Washington, DC

Purpose: We have developed a noninvasive local coil for both high-resolution and large-field-of-view (FOV) imaging of the pelvis.
Methods: The coil was constructed with two latchable loops, each with distributed capacitance, connected in parallel and inductively coupled to the RF source with a transformer. The two loops are wrapped around the superior portion of the thigh, with tune-match circuitry mounted in the cushion base of the coil. S/N and image homogeneity measurements were made by using ROI analysis in all three planes over a 16-cm spherical region.
Results: Body coil and pelvic coil S/N values were compared by using a 20-cm spherical phantom, demonstrating a 5–6-fold improvement in S/N. Using spin- and gradient-echo sequences, pelvic coil RF homogeneity was comparable with that of the body coil in all three planes. The pelvic coil provided superior small-FOV T1- and T2-weighted images of the prostate and the uterus. Sufficient coverage adds to the coil's versatility. This enables total pelvic imaging without changing coils: (1) large-FOV screening for lymphadenopathy and (2) high-resolution small-FOV studies for local tumor staging. This improvement in S/N allows 15-cm-FOV pelvic images with an in-plane spatial resolution of 1 × 1 mm and contiguous 3-mm sections.
Conclusion: This coil design combines advantages of body coil and high-resolution endorectal coil imaging with improved patient comfort. Clinical trials are under way in patients with prostate carcinoma and cervical cancer to determine the clinical efficacy of this device.

417 • 11:30 AM
Dynamic MR Perfusion Studies with Paramagnetic and Superparamagnetic Contrast Agents for Early Detection of Cerebral Ischemia
W Reith, M Forsting, H Vogler, W Hacke, K Sartov
Department of Neuroradiology, University of Heidelberg Medical School, Heidelberg, Germany

Purpose: Further improvement is needed in early radiologic diagnosis of cerebral ischemia. Such an improvement would likely influence the strategies of aggressive thrombolytic therapy. The aim of our study was to evaluate the usefulness of T2*-weighted FLASH sequences when combined with intravenous (IV) administration of para- and superparamagnetic contrast agents in the early phase of cerebral ischemia.
Methods: Focal cerebral ischemia was induced in 10 male Wistar rats by using an established model of transvascular occlusion of the right middle cerebral artery (MCA). Within 60 min after the onset of ischemia, all animals were examined on a 2.0-T experimental MR imager. First, conventional T2-weighted spin-echo images were obtained in all animals; then a fast T2*-weighted FLASH sequence was used after bolus injection of Gd-DTPA (0.3 mmol Gd/kg) to acquire 20 images within 32 sec. Five minutes later, this protocol was repeated to study the effect of superparamagnetic iron particles (0.03 mmol Fe/kg). In each animal, MR findings were correlated with microradiographic studies of the vascular occlusion pattern.
Results: Conventional T2-weighted spin-echo images were normal in all animals. FLASH images showed a marked decrease in signal intensity in the nonischemic hemisphere. Time-density curves obtained over this hemisphere and analyzed on an Apple Macintosh system gave a physiologic circulation time for the contrast medium, with a signal decrease first appearing 4 sec after injection. By comparison, in none of the animals did a signal alteration occur over time in the territory of the occluded right MCA. These findings were identical after the administration of the paramagnetic substance and of the superparamagnetic substance. Microradiographic studies showed complete vessel occlusion in the territory of right MCA.
Conclusion: The combination of fast T2*-weighted FLASH sequences with intravenous bolus application of paramagnetic contrast material allows early detection of cerebral perfusion deficits. This method can be readily

used on most existing MR systems, since it does not require hard- or software changes or the use of new superparamagnetic contrast agents.

418 • 11:40 AM

Ultrafast Kinematic MR Imaging of the Knee: Increased Sensitivity with a Quadriceps Loading Device

SM Brown, LR Muroff, WG Bradley, DJ Atkinson
University Community Hospital, Tampa, FL

Purpose: Patellofemoral malalignment and tracking abnormalities are a common cause of knee pain that can be difficult to detect solely by clinical examination. This entity ultimately leads to chondromalacia patellae and arthrosis. We developed an ultrafast technique to perform biplane kinematic MR imaging of the knee with a quadriceps loading device that accurately delineates patellofemoral malalignment and tracking abnormalities.
Methods: Five normal volunteers (10 knee joints) and 19 patients (37 knee joints) with patellofemoral symptoms and clinically suspected tracking problems were studied with kinematic MR imaging prior to and, in some cases, after a lateral release or other realignment procedure was performed. MR imaging was performed at 1.5 T with a curved surface coil. The TurboFLASH pulse sequence was used with a TR of 6.5 msec, TE of 3 msec, flip angle of 10° section thickness of 10 mm, FOV of 250 mm, and 100 × 128 matrix. Biplane acquisition was accomplished by interleaving sections acquired in the axial and sagittal planes. Each knee was imaged separately as the patient actively flexed and extended the knee while lying prone in the magnet. Unloaded studies were obtained in all cases. In all five normal volunteers (10 knees) and 20 symptomatic knees, the study was repeated with quadriceps loading. Total acquisition time was 17 seconds per knee.
Results: The loaded technique demonstrated a higher percentage (100%) of tracking abnormalities in 20 symptomatic patellofemoral joints than the unloaded techniques (75%) or clinical examination (89%). Both loaded and unloaded techniques were more specific than clinical examination.
Conclusion: Ultrafast kinematic MR imaging performed with a quadriceps loading device is more sensitive and specific than unloaded MR techniques. The biplanar technique allows rapid and accurate assessment of the patellofemoral relationship in patients with suspected tracking problems. In our experience, this technique accurately delineates patellar malalignment and tracking abnormalities that can be difficult to detect clinically.

419 • 11:50 AM

Echo-Planar Imaging with Conventional Imaging Gradients

X Wan, GT Gullberg, DL Parker, WL Davis
Department of Radiology, University of Utah School of Medicine, Salt Lake City, UT

Purpose: The single-shot echo-planar imaging (EPI) technique requires a rapid switching gradient field that is not always available on most clinical machines. The biggest problem of the standard gradient coil on most imagers is the long rise time. In most cases, data are collected only from the flat part of the readout gradient, while the ramping time is wasted. Turning on the data acquisition window during both the ramping and flat part of the readout gradient allows data to be acquired continuously. Data obtained during the ramping period fills k space nonequidistantly with a "sawtooth" pattern. Interpolating these data to the equidistance grid in k space makes efficient use of ramping time.
Methods: Imaging was performed with a standard GE 1.5-T Signa system. Data were collected at the maximum rate of 125 kHz or 8 μsec per IQ pair. The rise time of the gradient coil from zero to full scale (1 G/cm) was 500 μsec. The data acquisition time for a 128 × 128 image matrix was 98 msec with partial k-space imaging. Cubic spline interpolation was used to interpolate the data taken during the ramping period. A nonlinear phase correction based on a reference image with no gradient in the blip direction was used to minimize the Nyquist ghosts caused by reversing the direction of every other readout gradient.
Results: The image data were acquired in 98 msec, which was about half of the time required for conventional EPI with the same hardware. Images were reconstructed with interpolated data and nonlinear phase correction.
Conclusion: The use of data taken during the ramping period makes the implementation of EPI possible on a standard imager without adding any special hardware.

420 • 12:00 PM

Importance of Parameter Selection in Rapid Heart Imaging with Electrocardiogram-triggered T2-weighted Turbo Spin-Echo Sequences

J Gieseke, KC Seelos, A von Smekal, M Reiser
Department of Radiology, University of Bonn, Bonn, Germany

Purpose: Electrocardiogram (ECG)-gated T2-weighted spin-echo (SE) technique offers potential for differentiating various pathologic processes in and around the heart, but conventional SE imaging is time-consuming and, in addition, the image quality is limited by motion artifacts. To overcome this problem, a new ECG-adapted fast spin-echo method, turbo spin echo (TSE), based on RARE (1) and MEMS (2), with reduced acquisition time and SE-like contrast, was used and optimized. To analyze the influence of physiologic circumstances on image quality, TSE was tested at different functional states of the heart.
Methods: In 10 healthy volunteers, signal- and contrast-to-noise ratios of different structures were compared for different parameter settings: Various effective TEs were held constant (45–160 msec), when the number of profiles per excitation (3–25) and echo spacings (12–30 msec) were changed. All measurements were performed at different R-peak delays (20–1,000 msec).
Results: Smaller echo spacing improved motion artifacts, but a signal decrease occurred between 16 and 20 msec. Signal decrease with a longer effective TR was measured, possibly related to a stronger T2 influence. The best image quality was obtained during diastole. The optimized ECG-gated TSE sequence used an effective TE of 90 msec and an echo spacing of about 13 msec.
Conclusion: First experiences with ECG-gated TSE imaging of the cardiovascular system indicates that it may replace conventional SE, widening the diagnostic possibilities with the distinctly reduced imaging time, low artifact susceptibility, and high signal-to-noise ratio. Optimal image quality can be obtained with small echo spacing, a diastolic trigger delay, and an effective TE that should be kept below 100 msec.
1. Hennig J, Nauerth A, Friedburg H. Magn Reson Med 1986; 3:823–833. 2. Mehlkopf AF, van der Meulen P, Smidt J. Magn Reson Med 1984; 1:295–297.
J. Gieseke is an employee of Philips Medical Systems.

WIP 3: MRI–Technical

MODERATORS: LP Clarke, PhD • J Illes, PhD

421 • 10:30 AM

Use of a Skip-Echo Hadamard Sequence for Localizing Cortical Activation to Visual Words

J Illes, J Gabrieli, D Rumelhart, MV Stone, SL Thompson-Schill, GH Glover
Department of Radiology, Stanford University, Stanford, CA

Purpose: To explore whether an efficient gradient-recalled-echo (GRE) sequence that exploits T2* contrast can be used to reveal regional cortical activation for language function.
Methods: Previous functional MR studies have demonstrated cortical localization of primary sensory and motor processes. In this study, we used a new Hadamard-encoded skip-echo sequence (Glover, SMRI, 1993) to measure cortical activation to visually presented word and nonword stimuli. Studies were performed on a 1.5-T imager with a 12.5-cm surface coil placed at the posterior extremity of the skull. Images (4 sections) were obtained with a TE of 39.5 msec and TR of 50 msec, with a section thickness of 7 mm and an intersection distance of 2.5 mm. Following the paradigm of Petersen et al (Science, 1990, 249:1041), real words and matched unpronounceable consonant strings were presented in an A-B design at a rate of 1 stimulus per second in 12 acquisitions. Subjects viewed the stimuli passively. Images were compared with paired *t* tests to detect significant regional differences between word and nonword conditions.
Results: In two subjects studied to date, significantly greater activation was seen in the word (vs nonword) condition in posterior left hemisphere regions. Results were consistent with both positron emission tomographic (PET) and clinical neuropsychological evidence for left hemisphere mediation of visually presented verbal information.
Conclusion: These results demonstrate that higher cognitive brain function can be localized efficiently and with high spatial resolution with MR imaging.

422 • 10:40 AM

Multisection Black Blood Angiography

JN Lee, AR Sanderson
Medical Imaging Research Lab, University of Utah, Salt Lake City, UT

Purpose: The goal was to develop a multisection method of black blood angiography that can cover a large field of view in a reasonable imaging time. Such a pulse sequence would be especially useful in the lower extremities, where phase-contrast methods cannot be sensitive to both high velocities and the low velocities in aneurysmal vessel segments, and time-of-flight methods tend to overestimate the degree of a stenosis because of intravoxel dephasing.
Methods: A fast spin-echo (FSE) pulse sequence was modified to apply a section-selective inversion pulse superior to the imaging section about 600 msec before image acquisition. The pulse was designed by using the Shinnar-Le Roux algorithm of John Pauly. The bandwidth and transition widths of the inversion pulse were chosen to null the signal of blood with a maximum velocity of 10 cm/sec and a minimum velocity of 1.33 cm/sec. Although higher instantaneous velocities are experienced during the cardiac cycle, the mean velocity of any 600-msec period is usually less than 10 cm/sec. The narrow transition width chosen requires a pulse length of 15 msec. Relaxation effects during the pulse are minimal because of the long T2 of blood.
Results: Black blood angiograms will be shown that are extracted from 60-section acquisitions by using a region-growing connectivity algorithm.
Conclusion: Multisection black blood angiography can achieve average acquisition times of 3 seconds per section, which is as fast as time-of-flight sequences. The 2–3-second TR necessary for inversion recovery is made possible by acquiring a large number of interleaved sections.

423 • 10:50 AM

Clinical Carotid MR Angiography Improvement with Optimized Fat Suppression Technique

J Mao, J Gauger, WD Bidgood, H Yan
Department of Radiology, University of Florida, Gainesville, FL

Purpose: To determine whether an optimized fat suppression technique significantly improves image quality for carotid MR angiography.
Methods: We have recently developed a fat suppression technique by optimizing the chemical shift selective presaturation pulse. This technique can uniformly suppress the inhomogeneously broadened fat signal without specific shimming for routine clinical imaging. The optimized pulse precedes the 3D FISP TOF sequence. Images are postprocessed with MIP. The duration of the pulse is 20 msec at 1.5 T (Siemens, Magnetom). TE is 7 msec and TR is 54 msec, with one spatial saturation pulse. The axial slab thickness is 12 cm. The coronal slab thickness is 6.4 cm. There are 64 partitions, and the matrix is 160 × 256. The FOV is 20 cm for axial and 26 cm for coronal imaging, and the flip angle is 20°. Imaging time is 9 minutes. A Siemens neck coil is used for axial imaging, and a transmit and receive neck coil is used for coronal imaging. Four volunteers participated in the study, and two experienced radiologists scored the images.
Results: Compared with conventional MR angiography techniques, our optimized fat suppression technique shows significantly improved image quality in carotid arteries. Compared with commercially available MR angiography techniques, which need four separate scans to image the whole carotid artery from aortic arch to the bifurcation along the axial direction, our technique needs only two separate scans to produce similar or even better image quality. An image of the entire carotid system is obtainable with coronal imaging.
Conclusion: By using the optimized fat suppression technique a significant improvement in image quality for carotid MR angiography is achieved.

424 • 11:00 AM

Three-dimensional Multislab Phase-Contrast Imaging

G Cao, DL Parker, WL Davis, DD Blatter
MIRL/Radiology Department, University of Utah Medical Center, Salt Lake City, UT

Purpose: To reduce noise, 3D phase-contrast (PC) images are often displayed as the product of the phase image and the magnitude image. Because vessel intensity in the magnitude image is a function of time-of-flight (TOF) effects, there may be significant signal loss for small vessels located deep within a 3D imaging region. In this study, we test the hypothesis that the acquisition of multiple, overlapping, thin 3D PC slabs can reduce TOF signal loss and improve small vessel visibility.
Methods: The MOTSA PC pulse sequence combines 3D multislab acquisition with the balanced 4-point PC technique. A comparison between standard 3D PC and MOTSA PC on a conventional GE Signa MR imager was

performed in two healthy volunteers under identical imaging conditions (same FOV, section thickness, flip angle, etc). We used 50% overlap between adjacent slabs and 32 sections per slab. To reduce imaging acquisition time, we also performed a comparison with 25% slab overlap.
Results: Some vessels, such as the middle cerebral artery, posterior cerebral artery, and transverse sinus, are more visible on the MOTSA PC image (maximum-intensity projection display). The signal is greater on some parts of the 3D PC images, but the signal deviation is also large due to signal decrease along the flow direction. The saturation effect in the 3D PC images is more obvious than we expected.
Conclusion: The vascular detail on MOTSA PC images is better than that obtained with the standard 3D PC technique.

425 • 11:10 AM
Cardiac-gated MR Angiography Studies of Pulsatile Flow: K-Space Strategies
A Franck, K Selby, RE van Tyen, D Saloner
Radiology Service, VA Medical Center, San Francisco, CA

Purpose: MR angiography methods typically acquire data without interruption and without reference to any physiologic signal. We have applied prospective cardiac gating to MR angiography of pulsatile flow while reordering the collection of k space to investigate whether an improvement in image quality may be obtained by synchronizing the acquisition of specific frequency components with high flow conditions.
Methods: Image appearance of flow through a cylindric tube was studied with both simulations and phantom measurements. Flow velocities were measured using laser Doppler velocimetry and MR imaging. Simulations and measurements were performed with different algorithms for the sequencing of the phase-encoding lines. These included (*a*) reordering of k space to minimize signal oscillations from multiple cardiac cycles and gating the acquisition of only (*b*) the low-order phase-encoding lines or (*c*) the high-order phase-encoding lines.
Results: Good correlation was found between simulations and phantom experiments. Reordering of k space (*a*) reduces ghosting but blurs vessel edges because of the broadened PSF. The (*b*) algorithm showed good contrast properties but poor edge definition. The (*c*) algorithm was expected to provide improved edge definition, but any improvement was obscured by the high-strength ghosting associated with the ungated low-order phase-encoding lines.
Conclusion: We found that an improved strategy is to gate the low-order phase-encoding lines to systole and, in the same cardiac cycle, to acquire the high-order phase-encoding lines in diastole. This permits us to obtain high-contrast studies with little increase in imaging time.

426 • 11:20 AM
Continuous Inversion of Inflow for Lower-Extremity Angiography and Perfusion Mapping
PD Bergey, AK Hoydu, DA Roberts, JS Leigh Jr
Department of Radiology, University of Pennsylvania, Philadelphia, PA

Purpose: This study addresses the feasibility of continuous inversion of inflow to assess blood flow to the distal lower extremity.
Methods: Volunteer subjects with no evidence of peripheral vascular disease were recruited for MR angiography and perfusion mapping. For both kinds of imaging, inflowing spins are continuously inverted (1) as they pass through an axial plane positioned near the knee (flow-labeled image) or ankle (mask image). A subtraction MR angiogram is obtained as the difference between flow-labeled and mask images acquired in a longitudinal plane in the region of the popliteal artery and its major branches. A perfusion image is the difference between the flow-labeled and mask images acquired in an axial plane equidistant between the two inversion planes.
Results: Angiograms of the popliteal trifurcation obtained by the continuous inversion technique were obtained in a fraction of the time required for conventional MR angiograms and show the vascular anatomy in comparable detail. Perfusion mapping is insufficiently sensitive to be useful in the resting state. Exercise or some other physiologic maneuver must be used to elevate tissue perfusion to detectable levels. With exercise, dilatation of deep veins in the calf is observed and is probably a correlate of increased total inflow.
Conclusion: Continuous inversion of inflow is practical for rapid peripheral angiography. As a technique for measuring perfusion, it has limited sensitivity but it may be able to detect the increase that occurs with exercise or another provocative test.
1. WT Dixon, LN Du, DD Faul, M Gado, S Rossick, Magn Reson Med, 3, 454 (1986).
This work was supported by National Institutes of Health grants RR02305 and HL07614.

427 • 11:30 AM
High-Resolution Phase-Contrast Sequence for Very Slow Flow
NJ Pelc, AM Norbash, A Shimakawa, DR Enzmann
Richard M. Lucas Center, Stanford University School of Medicine, Stanford, CA

Purpose: Our goal was to develop a reliable method for imaging and quantifying flow in ventriculoperitoneal (VP) shunts used in hydrocephalus. The challenging requirements include (*a*) sensitivity to very slow flow ($v_{enc} < 0.5$ cm/sec) of long T1 fluid, (*b*) high spatial resolution (≤ 0.25 mm), and (*c*) immunity to B_0 inhomogeneity outside the skull, where the shunts are located. Conventional phase-contrast sequences fail due to low cerebrospinal fluid (CSF) signal secondary to inhomogeneity and saturation effects.
Methods: A spin-echo approach was selected for immunity to B_0 inhomogeneity. The RF portion of the sequence is α-π-π to maximize the signal for long T1 CSF. The timing of the RF pulses produces two asymmetric spin echoes; only the second is used. Bipolar flow encoding between the 180° pulses is used. Typical parameters are v_{enc} = 0.2–0.4 cm/sec, α = 45°, TR = 400–500 msec, 256 × 256 matrix, and 3–4 minute imaging time. Flow through shunts of various designs was measured in vitro. Hydrocephalus patients with functioning and nonfunctioning shunts were imaged.
Results: The method simultaneously achieved strong flow encoding and high spatial resolution. The in vitro accuracy for < 0.2 mL/min flow through < 1 mm shunts was ≈ 0.03 mL/min. Results in patients indicate that with careful technique, even VP shunt flow less than the CSF production rate can be measured.
Conclusion: Phase-contrast spin-echo MR imaging is well suited for measurements of very slow flow with high spatial resolution, such as in VP shunts.
A. Shimakawa is an employee of GE Medical Systems.

428 • 11:40 AM

Physiologic Pressure Measurement with MR

SN Urchuk, DB Plewes

Department of Medical Biophysics, University of Toronto, Sunnybrook Health Science Centre, Toronto, Ontario, Canada

Purpose: A method for determining pressure gradients from dynamic measurements of fluid velocity is presented.

Methods: The approach is based on an evaluation of shear and local inertial forces in measurements of fluid velocity. The difference in these quantities—which are proportional to the Laplacian and temporal derivative of the fluid velocity (neglecting convective acceleration)—yields the pressure gradient. Spatial averaging was used to obtain a robust estimate of the pressure gradient in the presence of noise. Numerical simulations and experimental measurements of fluid velocity were used to investigate the feasibility of the technique in the presence of noise. Velocity measurements were performed by using a temporally gated phase-contrast (PC) pulse sequence. As a control, direct measurements of the pressure gradient were obtained with pressure transducers.

Results: Numerical simulations predict that estimation of physiologic pressure gradients with a precision of 0.005 mm Hg/cm are feasible with clinical PC pulse sequences by using temporal resolution on the order of 20 msec, spatial resolution of 0.5–1.0 mm for tubes greater than 4.0 mm in diameter and signal-to-noise ratios of at least 25. These findings are supported by the agreement of pressure gradients derived from MR velocity data and measurements made with pressure transducers.

Conclusions: The results indicate that noninvasive measurement of pressure gradients is feasible and suggest that measurement of absolute pressure with a knowledge of pressure wave propagation velocity may be a practical goal. Such a technique should provide valuable information on hemodynamic function.

429 • 11:50 AM

Velocity-Encoding 2D Cine Phase-Contrast Imaging for Quantifying Peripheral Artery Disease

JB Weigele, AH Stolpen, PD Maldjian, GA Holland, ML Schiebler

Department of Radiology, Hospital of the University of Pennsylvania, Philadelphia, PA

Purpose: To evaluate the ability of MR-derived arterial velocity measurements in quantifying hemodynamically significant peripheral vascular disease.

Methods: MR studies were performed with a 1.5-T magnet (Signa, GE) with an extremity coil and a velocity-encoding 2D cine phase-contrast technique. Popliteal arteries of 5 normal subjects and 4 superficial femoral or popliteal arteries of patients with proximal arterial stenoses or complete occlusions have been studied. Arteries were imaged in the axial plane, with a 256 × 256 matrix, 2 signals averaged, venc = 100 cm/sec, 16 cardiac phases, and 16-cm field of view. Mean and peak velocities were determined for each phase. The 3D plots of cross-sectional velocity profiles were displayed versus time with an image analysis program (IDL, Research Systems). MR velocity results were correlated with duplex Doppler ultrasound results in healthy individuals. In patients, MR-derived velocities were correlated with results of noninvasive studies, MR angiograms, and conventional angiograms.

Results: In 5 healthy subjects, MR-derived velocity waveforms were triphasic and correlated well with Doppler-derived waveforms. The peak phase mean velocity was 28.6 cm/sec ± 2.4. Cross-sectional velocity profile plots were characteristic of peripheral artery pulsatile flow. The patients with proximal stenoses or occlusions demonstrated monophasic or biphasic waveforms, with decreased rates of change in velocity. Peak velocities were diminished and agreed with the severity of proximal occlusive disease.

Conclusion: MR-derived velocity measurements can quantify the hemodynamic significance of arterial stenoses and occlusions and should enhance the MR evaluation of peripheral vascular disease.

430 • 12:00 PM

Cine Phase-Contrast Flow Volumetry in Patients with Portal Venous Hypertension: High Association of Variceal Hemorrhage with Hyperdynamic Portal Flow

DJ Burkart, CD Johnson, RL Ehman

Diagnostic Radiology, Mayo Clinic, Rochester, MN

Purpose: There is a need for a test that can accurately identify patients at high risk for variceal hemorrhage so they can receive appropriate therapy. The purpose of this study was to quantitate portal venous flow in patients with portal venous hypertension and assess its potential for predicting variceal hemorrhage.

Methods: Thirty-two patients (19 men, 13 women) with portal venous hypertension and endoscopically proven esophageal varices were evaluated with cine phase-contrast (CPC) techniques. Flow measurements in the main portal vein were obtained and correlated with the presence of variceal hemorrhage within 2 years of the MR examination.

Results: Low (hypodynamic) flow of 7.2 mL/min · kg ± 4.1 was present in 22 of 32 patients, while high (hyperdynamic) flow of 25.4 mL/min · kg ± 5.5 was present in 10 of 32 patients. The portal venous flow rate was significantly associated with variceal bleeding by univariate ($P = .001$) and multivariate analysis ($P = .004$). Significant univariate associations were found between the presence of hemorrhage and the characteristics of variceal grade ($P = .030$) and Child's classification ($P = .001$). Child's classification was also associated with portal venous flow ($r = -0.51$, $P = .003$).

Conclusion: Quantitative MR flow volumetry demonstrated that hyperdynamic portal venous flow was highly associated with variceal hemorrhage in this patient series. The results suggest that the potential utility of CPC flow measurements for predicting variceal hemorrhage should be evaluated in a prospective study.

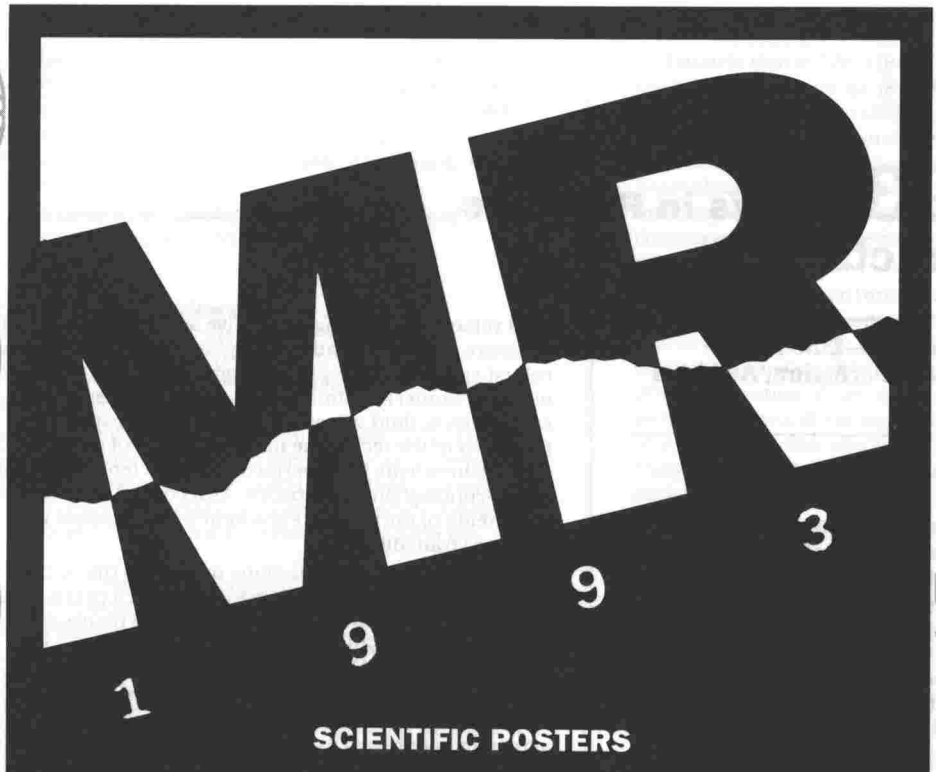

SCIENTIFIC POSTERS

The Scientific Poster Exhibits offer **SMRI** attendees an opportunity to examine and discuss scientific material in a more intimate atmosphere.

Discussion periods, moderated by individual Scientific Poster presenters, are scheduled daily throughout the Meeting. A schedule of the discussion times follow:

Section: **Physics I: Flow, Motion, Perfusion, Artifacts**
Day, Date: Sunday, March 28
Time: 12:15 PM - 1:30 PM
P039-P044

Section: **Clinical MRI: Head, Spine, Body**
Day, Date: Monday, March 29
Time: 12:30 PM - 1:30 PM
P141-P151

Section: **Contrast Agents, Spectroscopy, Other Nuclei**
Day, Date: Wednesday, March 31
Time: 12:15 PM - 1:00 PM
P336-P339

SOCIETY FOR MAGNETIC RESONANCE IMAGING

SMRI '93 Works in Progress

Poster Abstracts

Sunday, March 28, 12:15 PM–1:30 PM
PHYSICS I: Flow, Motion, Perfusion, Artifacts

Posters P039–P044

P039

MR Imaging of Excised Vascular Tissue

AJ Martin, RM Henkelman

Department of Medical Biophysics, University of Toronto, Sunnybrook Health Science Centre-Research, Toronto, Ontario, Canada

Purpose: The ability of MR angiography to locate regions of stenosis has been well demonstrated. MR techniques, however, have the potential to elucidate additional information on the extent and composition of the plaque causing the stenosis. This investigation assesses the ability of MR to segregate normal arterial anatomy and characterize atherosclerotic plaque.

Methods: A series of femoral arteries were excised during autopsy and subsequently imaged on a 1.5-T Signa (General Electric, Milwaukee) imager. A small-bore gradient insert was used, allowing peak gradient strengths of 3 G/cm. Arteries were immersed in a proton-free solution of $C_2Cl_3F_3$ and placed within a 4.2-cm-diameter solenoidal coil for imaging. High-resolution (voxel dimensions of 156 × 156 × 1,000 μm) images were then acquired with a wide array of contrast and subsequently compared with histologic findings.

Results: High-resolution axial images of nondiseased femoral arteries exhibit a banded structure that is most evident on T2-weighted images. A bright intimal layer is separated from the media by a narrow dark band that appears to correspond to the internal elastic laminae. The adventitia is dark, with some bright periadventitial fat. Diseased tissue tends to have a more variable appearance; however, contrast between the fibrous cap and necrotic core of atherosclerotic plaques was noted in several instances.

Conclusion: MR imaging is capable of providing detailed anatomic maps of the arterial wall and atherosclerotic plaque. Further analysis of the appearance of severely diseased arteries is necessary.

P040

Physiologic Pressure Measurement with MR

SN Urchuk, DB Plewes

Department of Medical Biophysics, University of Toronto, Sunnybrook Health Science Centre, Toronto, Ontario, Canada

Purpose: A method for determining pressure gradients from dynamic measurements of fluid velocity is presented.

Methods: The approach is based on an evaluation of shear and local inertial forces from measurements of fluid velocity. The differences in these quantities, which are proportional to the Laplacian and temporal derivative of fluid velocity (neglecting convective acceleration), yield the pressure gradient. Spatial averaging was used to obtain a robust estimate of the pressure gradient in the presence of noise. Numerical simulations and experimental measurements of fluid velocity were used to investigate the feasibility of the technique in the presence of noise. Velocity measurements were performed with a temporally gated phase-contrast pulse sequence. As a control, direct measurements of the pressure gradient were obtained with pressure transducers.

Results: Numerical simulations predicting that estimation of physiologic pressure gradients with a precision of 0.005 mm Hg/cm are feasible with clinical phase-contrast pulse sequences with temporal resolution on the order of 20 msec, spatial resolution of 0.5–1.0 mm for tubes greater than 4.0 mm in diameter and signal-to-noise ratios of at least 25. These findings are supported by the agreement of pressure gradients derived from MR velocity data and measurements made with pressure transducers.

Conclusion: These results indicate that noninvasive measurement of pressure gradients is feasible and suggest that measurement of absolute pressure through a knowledge of pressure wave propagation velocity may be a practical goal. Such a technique should provide valuable information on hemodynamic function.

P041

Transport-induced Adiabatic Fast-Passage Bolus Tagging for Measurement of Change in Cardiac Output

AK Hoydu, PD Bergey, DA Roberts, JS Leigh

Department of Radiology, University of Pennsylvania, Philadelphia, PA

Purpose: To measure in vivo sensitivity of transport-induced adiabatic fast-passage bolus tagging (1) to physiologic intervention known to raise cardiac output (CO).

Methods: Cardiac-gated images demonstrating flow velocities in the aorta were obtained with a gradient-echo sequence preceded by an 8-msec constant amplitude (B_1 = 120 Hz) RF pulse applied in the presence of a gradient in the frequency-encoding direction. The sequence was repeated to produce 30 images at 32-msec intervals throughout the cardiac cycle. Two signals were averaged in 4.3 minutes. A healthy volunteer was studied on a 1.5-T Signa MR system before and 20 and 30 minutes after consuming a well-balanced meal. Velocities were calculated as displacement of band divided by time between center of inversion and echo acquisition. Blood flows were obtained by integrating velocity over the aortic cross-sectional area, and stroke volumes (SV) were calculated as net flow over the cardiac cycle.

Results: Baseline data: SV = 78.7 mL, heart rate (HR) = 55 bpm, and CO = 4,329 mL/min. Twenty minutes postprandially, HR increased by 9% (60 bpm), SV increased by 23% (96.9 mL), and CO increased by 34% (5,814 mL/min). Thirty minutes postprandially, HR decreased but

was still elevated above resting HR by 5.5% (58 bpm), SV continued to increase to 34% above baseline (104.4 mL), and CO was 40% above baseline (6,055 mL/min).

Conclusion: We have demonstrated that transport-induced adiabatic fast-passage bolus tagging can measure physiologic changes in blood flow in vivo. The measured changes are consistent with previous findings.

1. WT Dixon, LN Du, DD Faul, M Gado, S Rossnick. Magn Reson Med, 3, 454 (1986).

This work was supported by National Institutes of Health grants RR02305 and HL07614.

P042

MR Imaging Evaluation of TIPS Patients

JB Weigele, PD Maldjian, AH Stolpen, GA Holland, L Dougherty, ZJ Haskal, CC Cope, ML Schiebler

Department of Radiology, Hospital of the University of Pennsylvania, Philadelphia, PA

Purpose: The TIPS procedure (transjugular intrahepatic portosystemic shunt) is gaining acceptance as an important therapy for symptomatic portal hypertension (variceal hemorrhage, intractable ascites). This study assessed the value of MR imaging for the evaluation of TIPS patients.

Methods: MR imaging was performed with a 1.5-T magnet (Signa, GE). There were 8 pre-TIPS and 7 post-TIPS MR studies. Sequences included axial spin echo (SE) in all cases, 2D time-of-flight MR angiography in 4 pre- and 2 post-TIPS studies, and velocity-encoding 2D cine phase contrast in 3 pre- and 2 post-TIPS studies. The 2D phase-contrast velocity measurements were validated with a flow phantom and in 11 healthy volunteers.

Results: SE imaging of TIPS patients demonstrated liver size and morphology, portal venous anatomy, and major collateral pathways. Large hemorrhoidal varices in one patient decreased dramatically following TIPS. In another, an unsuspected postprocedural pseudoaneurysm was detected. Pre-TIPS MR angiograms demonstrated the three-dimensional relationship of the portal and hepatic veins and confirmed patency, valuable for planning the TIPS procedure. Pre- and post-TIPS MR angiograms demonstrated major collateral pathways and their therapeutic response. Normal MR-derived fasting portal vein volume flow rate averaged 1,170 ± 247 mL/min. MR and Doppler peak velocities correlated well. Pre-TIPS patients demonstrated a hepatopedal flow rate below normal volume flow rate. Post-TIPS patients had an increased portal volume flow rate.

Conclusion: MR imaging demonstrates three-dimensional vascular and hepatic morphology, important for planning and follow-up of the TIPS procedure. Portal vein flow measurements should provide useful physiologic information.

P043

Differentiation of Intracardiac Masses by Perfusion Pattern with Ultrafast MR Imaging at 0.5 T

A von Smekal, KC Seelos, J Gieseke, W Fehske, M Reiser, HJ Biersack

Department of Nuclear Medicine/Radiology, University of Bonn, Bonn, Germany

Purpose: To investigate the potential of ultrafast dynamic contrast-enhanced (Gd-DTPA) MR imaging sequences for optimizing differentiation of intracardiac masses by their perfusion pattern.

Methods: Twenty patients with unclear intracardiac masses, referred from the echocardiography laboratory were studied (0.5 T, T5 Philips Gyroscan). Selectively angulated single- or multisection dynamic electrocardiogram-gated turbo field echo (FE) sequences were acquired with TR = 10 msec and TE = 5 msec, flip angle = 30°, inversion prepulse T1-weighted contrast enhancement, 1 turbo FE shot, FOV = 350 mm, rectangular FOV = 65%, and matrix size = 128 × 96. Time resolution was less than 1 second for single-section acquisition of 64 contiguous dynamic images. Following the second dynamic image, a Gd-DTPA (0.1 mmol/kg) bolus was intravenously injected. Multiple ROIs were positioned in the masses, heart chambers, and myocardium. For each ROI time-intensity curves were calculated. Data were regionally compared. Results were compared with echocardiography.

Results: Intracardiac tumors (7/20 patients) and vital myocardium showed signal intensity increases over time, due to vascularization. Thrombus did not show increases in signal intensity (13/20). Even in mixed structures (3/20) identification of thrombotic components, tumor, and perfused myocardium was easily done. In echocardiography, differentiation was sometimes inconclusive, especially in mixed structures. Pathology or follow-up examinations after therapy confirmed the MR diagnosis.

Conclusion: Dynamic perfusion imaging allows clear differentiation of intracardiac tumors, thrombus, and perfused myocardium by their perfusion pattern. This technique has the potential to become the method of choice for differentiation of echocardiographically uncertain intracardiac masses.

P044

Clinical Applications of a Miniflex, Wraparound Local Coil for MR Imaging

FG Shellock, RS Hashoian, JH Mink, CJ Schatz, A Deutsch

Tower Imaging and UCLA Medical Center, Los Angeles, CA

Purpose: To determine the clinical applications of a newly developed, miniflex, wraparound local coil for MR imaging.

Methods: Thirty-four patients were imaged with a 1.5-T MR imager and a miniflex (3.5 × 5.0 inches), wraparound local coil (12 orbits, 4 patellae, 6 hands, 7 wrists, 5 forefeet). For most cases, images were compared with those obtained by using conventional local coils (ie, head coil, extremity coil, single or dual 5-inch circular coils) and the same section locations and MR imaging parameters.

Results: In general, the image quality of the MR studies acquired with the miniflex, wraparound local coil was comparable with or better than that obtained with the conventional local coils. Furthermore, the miniflex coil was technically easier to use for MR imaging, especially for specific clinical applications, including MR examinations of the hand, wrist, and forefoot.

Conclusion: The miniflex, wraparound local coil may be used for a number of important clinical MR imaging applications. This local coil offers definite advantages over existing conventional local coil technology.

Monday, March 29, 12:30 PM–1:30 PM
CLINICAL MRI: Head, Spine, Body

Posters P141–P151

P141

Analysis of Functional Brain MR Images with Z Maps

D Le Bihan, P Jezzard, R Turner, CA Cuenod, T Zeffiro
Diagnostic Radiology Department, Clinical Center, National Institutes of Health, Bethesda, MD

Purpose: MR imaging is now used to detect local changes in signal intensity caused by functional brain activation. Such changes, however, are small, so that sophisticated subtraction algorithms may be required to distinguish activated areas. We propose such an algorithm based on calculation of a statistical Z variable.

Methods: Volunteers performed visual, motor, language, and auditory tasks at 1.5 and 4 T. Blood oxygenation contrast was monitored with either EPI or SPGR sequences. The paradigm consisted of stimulation episodes separated by rest. Activation maps $Z(x, y)$ were calculated on a voxel-by-voxel basis as a statistical variable Z:

$$Z(x,y) = \left[\frac{\sum_{j=1}^{n} J_j(x,y)/n}{\sum_{i=1}^{m} I_i(x,y)/m} - 1 \right] / SD,$$

in which the mean of n images (typically 5) acquired during stimulation $J(x, y)$ was compared with the mean of m "rest" images $I(x, y)$ (typically 5). SD is the normalized standard deviation of the measurements. These Z maps, which represent activation significance level are color coded with a rainbow scale and overlaid on a gray-scale high-resolution anatomic image for accurate structural assignment.

Results and Conclusion: Qualitatively activated regions were clearly identified on Z maps and correlated well with brain localization expected for each specific task. Furthermore, these Z maps allowed different regions and tasks to be compared on a semiquantitative basis within each individual (eg, actual stimulation vs imagined stimulation).

P142

Functional Brain Imaging with Conventional Gradient-Echo Sequences at 1.5 T

RT Constable, G McCarthy, T Allison, AW Anderson, JC Gore
Department of Diagnostic Radiology, Yale University, New Haven, CT

Purpose: To demonstrate that functional brain MR imaging may be performed at high resolution with conventional gradient-echo imaging techniques at 1.5 T. To date, most activation studies have been performed either at high field strength or by using echo-planar imaging. Since these are not widely available, it is important to investigate whether activation studies may be performed with conventional sequences at 1.5 T.

Methods: We demonstrate that visual, motor, and sensory cortex activation may be measured with a flow-compensated gradient-echo sequence ($\alpha = 40°$, TE = 45 msec, TR = 120 msec, FOV = 40 cm, section thickness = 7 mm, 256 × 128 matrix, 2 signals averaged). Up to 20 pairs of baseline and activation images were collected and a Student t test was used to determine which pixels demonstrated a statistically significant (.002 level) change in signal intensity.

Results: The percent change in signal intensity in the visual cortex, on stimulation with flashing lights, ranged from 3.7% to as high as 12.3%. For the motor cortex, using a finger-flexing task, the change was approximately 4%. For the sensory cortex, using electrical stimulation, the changes were smaller.

Conclusion: Brain activation may be measured with high resolution by using a conventional gradient-echo imaging sequence at 1.5 T. Subtraction of the baseline from the activation images is insufficient to accurately localize the activated region because of misregistration problems and/or motion artifacts. Paired baseline and activation images must be processed with a Student t test to determine statistically significant signal differences.

P143

Quantitative Comparison of Conventional and Fast Spin-Echo T2-weighted MR Imaging Evaluation of Myelination

DWW Shaw, E Weinberger, J Tsuruda, S Astley
Department of Radiology, Children's Hospital and Medical Center, Seattle, WA

Purpose: The process of myelination results in changing tissue contrast with conventional spin-echo (CSE) imaging. The mechanism for tissue contrast is more complex with fast spin-echo (FSE) imaging, with multiple echoes used to form a composite image. Quantitative analysis of relative signal intensity (SI) on T2-weighted (T2W) images between gray matter (GM) and white matter (WM) in the developing brain was performed by comparing percent contrast of these two tissues with CSE and FSE.

Methods: Cranial MR imaging (1.5T, GE Signa) was performed in 20 patients (1–44 months old) with both CSE and split-echo-train FSE sequences. SI of equal-size areas of WM and GM were measured at four comparison locations in addition to background measurements. Percent contrast was calculated and statistical analysis was performed with the Wilcoxon signed-ranks test.

Results: At over 10–15 months of age, mean percent contrast was significantly greater with FSE sequences. At under 10 months of age, percent contrast was better with CSE sequences, except in the cerebellum (where WM myelination is most advanced).

Conclusion: With myelination, on T2W sequences, WM is initially hyperintense and becomes isointense and subsequently hypointense to GM, although compared with CSE images, WM appears more hypointense to GM on FSE images. Consequently, myelination appears slightly advanced with FSE imaging relative to standards based on CSE imaging. This difference is probably at least in part due to magnetization transfer, which is greater in WM. Evaluation of magnetization transfer changes during myelination is currently under way to determine the extent of its effect on FSE imaging.

P144

Functional MR Mapping of Auditory Cortex

R Turner, D Le Bihan, P Jezzard, TA Zeffiro, JN Giedd
Clinical Center, National Institutes of Health, Bethesda, MD

Purpose: Gradient-echo imaging, especially gradient-echo EPI, has been successful (Kwong, Ogawa, Bandettini) in detecting local changes in blood oxygenation caused by functional activation in the human brain. We attempted to determine regions of activation in the temporal lobe resulting from auditory stimulation, using gradient-echo EPI.

Methods: Measurements were made with 1.5- and 4-T whole-body MR imaging systems, with the same local z-gradient coil and special EPI software. Images had a

16-cm FOV, with a matrix of 64 × 64, and section thickness of 5 mm, taking 41 msec to acquire an image at 4-T (TE, 25 msec) and 36 msec at 1.5 T (TE, 40 msec). Up to 64 repetitions of each of four contiguous sagittal sections were obtained, spanning the temporal lobe. Subjects reported that the auditory stimulus, a repetitive single musical note ("G," 1,680 Hz) was easily discernible from MR noises, despite the interference of the loud buzz produced by the EPI sequence and the use of ear plugs. During the 3-minute imaging time, periods of 30 seconds of rest and 30 seconds of auditory stimulation were alternated. With the last 6 images in the initial rest period used as a control, z maps were constructed showing the image difference (stimulated − control) in units of the standard deviation of each pixel.

Results: Significant intensity changes corresponding to the periods of auditory stimulus were observed in several regions in the superior temporal lobe.

Conclusion: The effect of auditory stimulation on human regional cortical blood oxygenation can be mapped with gradient-echo EPI.

P145

Efficient Skip-Echo Hadamard Sequence for Brain Activation Studies

GH Glover, J Gabrieli, J Illes, W Newsome, D Rumelhart, M Shadlen, B Wandell
Stanford University Medical Center, Stanford, CA

Purpose: To develop an efficient gradient-recalled-echo (GRE) sequence that exploits T2* contrast for cortical brain activation studies.

Methods: Increased oxygenation demand in cortex undergoing neuronal activation results in reduced paramagnetic deoxyhemoglobin levels, with concomitant regional increase in T2*. Previous work utilized long TE GRE sequences, which are inefficient because of long TR. Skip-echo sequences, which have TE > TR, have been recently described but are single section. We have developed a Hadamard-encoded skip-echo sequence that provides volume acquisition (4 sections) with good S/N for functional brain studies. The technique alternately excites 4 planes in two Hadamard pairs to provide S/N approximately twice that of a single-section method. The resulting TE/TR of 39.5/50 msec gives good activation contrast with high efficiency (33% A/D duty cycle). Motion artifacts are addressed by a postprocessing filter that differentiates activation contrast from artifacts on the basis of spatial and temporal characteristics. We are also investigating correction of the raw data with a navigator echo acquired with no time penalty.

Results: The new sequence has been applied to activation studies with a conventional 1.5-T clinical imager, using motor and photic stimulation paradigms, as well as to cognitive (eg, word/nonword) tasks. Contrast changes of 4%–10% have been observed with the sensory tasks. The motion correction methods diminish pulsatility artifacts.

Conclusion: Neuronal stimulation studies are performed efficiently on a conventional 1.5-T imager with the technique. Motion correction methods enhance the reliability of the results.

P146

Distinctive Marrow MR Imaging Patterns in Patients with Chronic Myeloid Leukemia Undergoing Allogeneic Transplantation

RL Soulen, V Reddy, JC Andersen, PE Morton, LL Sensenbrenner, WG Negendank
MR Center, Wayne State University/Harper Hospital, Detroit, MI

Purpose: To compare the marrow MR imaging patterns in patients with chronic myeloid leukemia (CML) undergoing allogeneic marrow transplants (ABMT) with the patterns of those with acute myeloid leukemia (AML) and myelodysplastic syndromes (MDS).

Methods: Forty-three patients (19 CML, 17 AML, 7 MDS), 26 female, 17 male, ages 9–54 years (mean, 34 years), underwent marrow MR imaging at 1.5 T with T1-weighted spin-echo and STIR sequences before and 1, 3, and 6 months and 1, 2, and 3 years after ABMT. All were in complete remission ($n = 39$) or early relapse ($n = 4$) before ABMT. Images were analyzed in blinded fashion for marrow pattern and signal intensity (SI) relative to that of muscle. These results were compared with histopathologic estimates of marrow iron stores (range, 0–4) determined independently. Groups were compared with the Student independent t test for dissimilar sample sizes.

Results: Prior to ABMT, CML patients all showed homogeneous marrow abnormality with low SI on T1 (mean, 1.41 ± 0.39) and high SI on STIR (mean, 1.38 ± 0.25) images; AML and MDS patients showed variable patterns; mean SIs on T1 images were 1.54 ± 0.62 and 1.39 ± 0.72, respectively; those for STIR were 0.74 ± 0.37 and 0.77 ± 0.14, respectively. T1 ratios did not differ between groups; STIR ratios in CML were significantly greater than in AML or MDS ($P < .05$). Estimated iron stores in CML were significantly lower than in AML or MDS ($P < .01$). Following ABMT, CML marrow could be consistently distinguished from AML or MDS by steady and earlier progression toward "normal" and higher STIR values up to 1 year. Iron stores changed little in CML but decreased significantly ($P < .05$) in AML and MDS during follow-up.

Conclusion: While the cause of the difference in pattern between CML and AML or MDS remains obscure, the difference in pre-ABMT iron stores can explain the difference in signal intensities and offers some insight into marrow remodeling and iron utilization after ABMT.

P147

Adenomyosis: Prospective Comparison of MR Imaging and Transvaginal Sonography

SM Ascher, LL Arnold, RH Patt, D Siker, KA Trumball, J Schruefer, RK Zeman, JA Simon
Department of Radiology, Georgetown University Medical Center, Washington, DC

Purpose: Published reports advocate MR imaging and transvaginal sonography (TVS) for the noninvasive diagnosis of adenomyosis. To date, these 2 modalities have not been compared. We prospectively evaluated MR imaging and TVS for the diagnosis of adenomyosis.

Methods: Eight women (mean age, 36 years) with unexplained pelvic pain and menorrhagia were evaluated. All subjects were imaged during the luteal phase of their cycle (days 20–26). MR imaging and TVS were performed within 3 months of each other. MR imaging was performed with a 1.0-T magnet (Siemens, Iselin) with T1-, T2-, T2 turbo- (T2-TSE), and post-Gd-DTPA T1-weighted spin-echo technique. Sonography was done with a 5.0-MHz transvaginal probe (GE, Milwaukee). MR and TVS images were prospectively analyzed in a blinded fashion by separate investigators for image quality (good, fair, and poor) and the presence of adenomyosis by using pub-

lished criteria. MR images, initially interpreted as individual sequences, were subsequently analyzed collectively. Pathology—endometrial biopsy or hysterectomy—was determind in all cases.

Results: All 8 patients had pathologic proof of adenomyosis. MR imaging and TVS correctly showed adenomyosis in 7 and 3 of the 8 patients, respectively. MR image quality was good in 6, fair in 1, and poor in 1. TVS image quality was good in 7 and fair in 1. T2 and T2-TSE sequences were comparable in displaying adenomyosis. Contrast-enhanced T1-weighted sequences were considered superior to unenhanced T1-weighted sequences for diagnosing adenomyosis but inferior to T2 and T2-TSE sequences.

Conclusion: Our preliminary results suggest that MR imaging is superior to TVS for diagnosing adenomyosis.

P148

3D Reconstruction of the Liver: Comparison of T1-weighted Spin-Echo and Contrast-enhanced TurboFLASH Images

J Cullingworth, J Ward, J Ridgway, AG Chalmers, PJ Robinson

St. James's University Hospital (MRI Unit), Leeds, England

Purpose: We explore the potential of 3D image reconstruction for improved segmental localization in patients who are candidates for hepatic resection. We evaluated both T1-weighted spin-echo and contrast-enhanced TurboFLASH images for 3D reconstruction of the liver to demonstrate segmental anatomy.

Methods: T1-weighted spin-echo (TR, 500; TE, 15) and contrast-enhanced TurboFLASH (TR, 135; TE, 4) images were acquired in 10 patients with a 1.0-T Siemens Magnetom 42SP. Segmentation of the liver, surface vessels, and lesions was performed on a 3D Allegro Workstation (ISG Technologies), and 3D color images of the liver were generated by a surface-rendering algorithm. Multiplanar reformatting was used to aid in identification of vessels on the axial images. Images were compared and scored independently by two radiologists to assess the demonstration of the hepatic and portal veins, lesion visibility, and the ability to segmentally localize.

Results: Results will be presented.

Conclusion: Initial experience suggests that 3D reconstruction aids in the demonstration of segmental anatomy.

P149

MR Arthrography versus CT Arthrography in Dislocation of the Shoulder

H Nobusawa, T Kushihashi, H Munechika, N Ohtuki, H Hirose, E Fujimaki

Department of Radiology, Showa University, Tokyo, Japan

Purpose: In patients with dislocation of the shoulder, both MR arthrography and CT arthrography are performed to evaluate Bankart lesion, Hill-Sachs lesion, and rotator cuff tear. If MR arthrography proves superior to CT arthrography in diagnostic quality, CT arthrography will not be needed.

Methods: Sixteen patients with dislocation of the shoulder underwent surgery. The surgical findings were correlated with imaging findings. T1-weighted MR images (TR/TE = 330–500/15) were obtained after intraarticular injection of diluted Gd-DTPA. CT arthrography was performed after intraarticular injection of iodinated contrast material and air. The diagnostic value of the studies was compared.

Results: Osseous Bankart lesions, nonosseous Bankart lesions, Hill-Sachs lesions, and rotator cuff tear were correctly diagnosed in 69%, 81%, 94%, and 100% of patients with MR arthrography and 67%, 73%, 93%, and 93% of patients with CT arthrography, respectively.

Conclusion: MR arthrography is superior to CT arthrography in the detection of nonosseous Bankart lesions and their extensions but is almost equal to CT arthrography in the evaluation of other shoulder lesions. CT arthrography is not needed if MR arthrography is performed in patients with dislocation of the shoulder.

P150

MR Imaging of Thickened Gallbladder Wall: Pathologic Correlation

K Ohgi, H Yoshimura, K Murata, T Furukawa, T Hayano, A Kohno, A Shigeta

Department of Radiology, Japanese Red Cross Medical Center, Tokyo, Japan

Purpose: To assess the usefulness of MR imaging in evaluating various causes of gallbladder (GB) wall thickening.

Methods: Eighty-one patients with GB wall thickening (acute cholecystitis, 34 cases; chronic cholecystitis, 26 cases; GB carcinoma, 12 cases; and adenomyomatosis, 9 cases) were examined with 1.5-T and 0.5-T superconductive MR systems. In addition to conventional T1- and T2-weighted SE images (81/81), routine (61/81) and dynamic (42/81) Gd-DTPA-enhanced images were also obtained.

Results: The thickened GB walls showed low signal intensity on T2-weighted images in cases of chronic cholecystitis without acute inflammation. In cases of acute cholecystitis, GB carcinoma, and adenomyomatosis, the thickened walls showed various patterns of high signal intensity on T2-weighted images. Among these three entities, layering patterns consisting of low- and high-signal-intensity bands on T2-weighted images were seen only in cases of acute cholecystitis. In pathologic correlations, the inner low-intensity band corresponded to the muscular layer, the outer high-intensity band corresponded to subserosal inflamed edema, and the thinner outer low-intensity rim corresponded to thickened serosa. On Gd-DTPA-enhanced images, the inner enhanced rims that pathologically corresponded to GB mucosa were not seen in cases of GB carcinoma.

Conclusion: MR imaging has the potential to provide valuable information in the differential diagnosis of thickened GB walls.

P151

MR Imaging Contrast Enhancement of Chymopapain-induced Loss of Proteoglycans in Cartilage: Model of Cartilage Degeneration

K Gersonde, Y Morita, C Raible

Fraunhofer-Institut für Biomedizinische Technik, St Ingbert, Germany

Purpose: Cartilage fine structures are shown by contrast-enhanced MR imaging via Mn^{2+}-proteoglycan (PG) electrostatic interactions (1). Mn^{2+} binding decreases T1 and T2 of water protons. Cartilage degeneration is accompanied by loss of PGs. Therefore, variation of Mn^{2+}-PG interactions due to a digestion of PGs by chymopapain and to variation in Mn^{2+} accumulation results in changes in contrast behavior on T1- and T2-weighted images of joint cartilage. Visualization of Mn^{2+}-PG interactions improves the diagnosis of degenerated joint cartilage.

Methods: T1- (250/18 at 4.7 T and 500/9 at 9.4 T) and T2-weighted (3,000/18 at 4.7 T) images and spatially resolved T1 and T2 measurements were performed with Biospec BMT 47/40 and MSL 400 in intact chicken knees after injection of activated chymopapain (10 mg in 1 mL)

into the joint space. Pixel resolution and section thickness were 70/150 μm and 280/2,000 μm, respectively. Optimum contrast was reached by injection of 1 mL of 1 mM Mn^{2+}, buffered in HEPES at pH 6.5.

Results: In the presence of Mn^{2+}, MR imaging differentiated spongious bone and five cartilage zones. Mn^{2+} shortened T1 and T2 in all cartilage zones. T1 and T2 of weight-bearing cartilage were shortest. Loss of proteoglycans, due to chymopapain digestion, was most severe in weight-bearing cartilage. This effect could be shown only in the presence of Mn^{2+}; T1 and T2 of weight-bearing cartilage became longer after loss of proteoglycans.

Conclusion: Small cationic paramagnetic complexes could provide MR imaging contrast agents for an improved in vivo diagnosis of degenerated cartilage.

1. Y Kusaka, W Gründer, H Rumpel, KA Dannhauer, K Gersonde: Magn Reson Med 24, 137–148 (1992).

Wednesday, March 31, 12:15 PM–1:00 PM
CONTRAST AGENTS, SPECTROSCOPY, OTHER NUCLEI

Posters P336–P339

P336

Spatially Localized 2D Correlation Spectroscopy with COSY SLIM

Y Yang, PC Lauterbur
Biomedical Magnetic Resonance Laboratory, University of Illinois, Urbana, IL

Purpose: This study demonstrates a method of obtaining spatially localized 2D correlation spectroscopy with SLIM (spectral localization by imaging). Two-dimensional COSY spectra from regions of arbitrary shape can be obtained by using a few phase-encoded spectroscopic signals with a priori information from high-resolution imaging.

Methods: Experiments were performed with a Sisco 4.7-T/33-cm imaging spectrometer, using a phantom consisting of 85% aqueous lactic acid and ethylene glycol (1 mL each) in two identical hollow plastic spheres immersed in D_2O. A total of 512 complex sampled data points were acquired in each of the 64 t_1 steps with 4 phase-cycled acquisitions. A set of 16 phase encodings (1 × 16 × 1) was used for 3D spatial localization by applying magnetic field gradients after the preparation pulses. The 16 phase-encoding steps were along the line of the centers of the two spheres. Routine spin-echo proton images were used to provide structure information for localization.

Result: The localized 2D COSY spectra of lactic acid and ethylene glycol of the entire phantom were well separated by SLIM processing of the 1 × 16 × 1 phase-encoding data set, and even with subsets of 1 × 12 × 1 and 1 × 8 × 1. There was almost no contamination between the two localized 2D spectra.

Conclusion: The COSY SLIM technique makes it possible to obtain 3D spatially localized COSY spectra from arbitrarily shaped regions by using only a few phase-encoding steps for spatial localization. The reduced phase-encoding requirement, compared with 3D CSI, makes it possible to acquire data in a reasonable time for practical applications.

P337

Animal Model of Muscle Denervation: an MR Imaging Study

D Suput, F Demsar, R Frangez, G Planinsic
Institute of Pathophysiology, School of Medicine, Ljubljana, Slovenia

Purpose: Models of neuromuscular block were developed by use of a commercial preparation of botulinum neurotoxin type A (Oculinum). MR imaging and spectroscopy were used to evaluate these models as possible correlates of human neurodegenerative disorders. Investigation of Oculinum-induced denervation also seems to be relevant because of the clinical use of *C botulinum* toxins.

Methods: Experiments were performed in male albino rats. Denervation was caused either mechanically (n = 9) or by intramuscular injections of Oculinum (n = 7). The integrity of neuromuscular transmission was evaluated by the force of muscular contractions, and muscle size was assessed by means of MR imaging. MR imaging measurements were performed with a 2.35-T Bruker imager. A spin-echo sequence with T1-weighted images (TR = 600 msec, TE = 34 msec) was used. P-31 spectra were measured with the same magnet.

Results: MR spectra show a shift of intracellular pH of 0.12 to 0.2 units (n = 4) toward a more alkaline value during the first two days after application of Oculinum. MR imaging of hind limbs revealed that the nerve crush and Oculinum-induced denervations cause reversible muscle atrophy. None of the models showed muscle degeneration characterized by fatty infiltrations, typical of human neurodegenerative disorders.

Conclusion: MR imaging enables reliable and continuous monitoring of muscle atrophy and regeneration after mechanically or chemically caused denervation. The signal intensity of the treated and untreated muscles were comparable, which might imply that the botulinum toxin–induced denervation does not induce fatty degeneration of the affected musculature.

P338

In Vivo Na-23 MR Spectroscopy of the Rat Heart

NB Butwell, N Bansal, MJ Germann, CR Malloy, AD Sherry
Department of Internal Medicine and Radiology, The Mary Nell and Ralph B. Rogers Magnetic Resonance Center, UT Southwestern Medical Center, Dallas, TX

Purpose: The accumulation of intracellular sodium (Na^+) during myocardial ischemia may play a critical role in the transition from reversible to irreversible injury. Shift reagent (SR)-aided Na-23 MR spectroscopy as a method of monitoring intra- and extracellular Na^+ has been used successfully in isolated myocardial cells and perfused hearts. The aim of this study was to evaluate the feasibility of intravenous administration of a recently developed SR, Tm-$DOTP^{5-}$, for the spectroscopic observation of myocardial intracellular Na^+ in vivo.

Methods: A 1-cm surface coil tuned to 53 MHz for Na-23 was placed over the left ventricle of a ventilated, open-chest rat. Next, 80 mM Tm-$DOTP^{5-}$ without added Ca^{2+} was infused while Na-23 spectra were acquired with a GE CSI Omega 4.7/40-cm spectrometer. By using a pulse width of 25 μsec and a TR of 345 msec, one-pulse Na-23 spectra were collected by means of 1,024 data points acquired over a sweep width of 3,000 Hz.

Results: Infusion of the SR produced a small decrease in mean arterial pressure. Na-23 spectra showed well-resolved peaks due to intra- and extracellular Na^+. The small unshifted peak is assigned to myocardial intracellular Na^+ while the larger shifted peak is probably due to interstitial and intracavitary Na^+.

Conclusion: Na-23 MR spectroscopy in combination with Tm-DOTP^{5-} in vivo may provide an excellent noninvasive technique for monitoring changes in intracellular Na^+ during pathophysiologic events and pharmacologic interventions.

P339

Relaxivity of Magnetites and Oxyhydroxides as a Function of Core Composition, Magnetic Field Strength, and Water Diffusion

JWM Bulte, J Vymazal, RA Brooks, C Pierpaoli, JA Frank
Diagnostic Radiology Department, National Institutes of Health, Bethesda, MD

Purpose: To obtain a better understanding of the precise effects of iron oxides on proton relaxation by studying variations in core composition, magnetic field strength, and water diffusion.

Methods: With a newly developed variable-field (0.05–1.5 T) relaxometer, T1 and T2 were measured in samples containing varying concentrations of gelatin for 9 different commercially available iron oxides: a polycrystalline silane-magnetite particle (SMP), 3 oligocrystalline dextran-magnetite particles (DMP), a monocrystalline DMP, a dextran-akaganeite particle (DAP), a dextran-ferrihydrite particle (DFP), and ferritin. The water diffusion coefficient of the gelatin samples was determined with diffusion MR imaging.

Results: In magnetites, 1/T1 decreased and 1/T2 increased (except for the 1-μm SMP) in proportion to gelatin concentration. This corresponded to a measured proportional decrease in the water diffusion coefficient. The 1/T1 value decreased and 1/T2 increased in proportion to particle size, except for SMP, for which the transverse magnetization decay did not follow a single-exponential function. The magnetic field depenedence of 1/T1 showed an identical behavior for all DMPs above 0.6 T, but large differences in 1/T1 were observed at lower magnetic fields. 1/T2 displayed a rapid increase followed by a plateau above 0.6 T. This behavior was a clear indication of magnetic saturation of the cores, which followed the Langevin magnetization function. From these curves, the magnetic moment of the magnetite domains was estimated to range from 0.8 to 6.3 × 10^4 Bohr magnetons. In oxyhydroxides, 1/T2 increased with increasing gelatin concentration for DFP and ferritin. The 1/T1 values for DFP and ferritin were similar and nearly constant over the entire field. DAP showed a striking increase in 1/T1 at high fields, presumably caused by an increased electron spin-lattice relaxation rate. The 1/T2 values for DFP and ferritin were similar, providing further evidence that the core of ferritin is pure ferrihydrite. For all oxyhydroxides, 1/T2 increased linearly with increasing field strength; the slope of the increase was 4 times greater for DAP than for DFP and ferritin.

Conclusion: The 1/T2 dependence on magnetic field is a reflection of core composition and core magnetization. The water diffusion coefficient can influence both 1/T1 and 1/T2 significantly. For iron oxides, present in tissues either as contrast agents or endogenous biominerals, these findings may aid in the interpretation of in vivo relaxivity and effect on MR imaging.

1993 ANNUAL MEETING COMMENTS

The 1993 Annual Meeting Organizing Committee would appreciate receiving your comments regarding the 1993 Annual Meeting in San Francisco. Those comments will be collated and forwarded to the 1994 Annual Meeting Organizing Committee for possible incorporation in next year's educational programming. While your comments may also be provided on the Evaluation/CME Accreditation Form distributed at each session, please let us know your thoughts regarding the following:

1. Which Program did you attend? _____

2. Did it meet its stated objectives?_____Yes ____ No . Why? _____

_____

_____

3. What should have been included in this Program that was not?_____

_____

4. What should hnve been excluded from the Program that was not? _____

_____

5. What Program revisions would you like to see implemented next year?_____

_____

_____

_____

6. General Comments _____

_____

_____

Please return this form to the **SMRI** Registration Area, Ballroom Level, of the San Francisco Hilton and Towers by Wednesday, March 31, or mail it to the **SMRI** Central Office at the following address:

Society for Magnetic Resonance Imaging
213 West Institute Place, Suite 501
Chicago, Illinois 60610 USA

Key To Abbreviations in Author Index

EP–educational program

#–proffered papers

P–scientific poster presentations

Key to abbreviations

EP–educational program
#–proffered papers
P–scientific poster presentations

WORKS IN PROGRESS AUTHOR INDEX

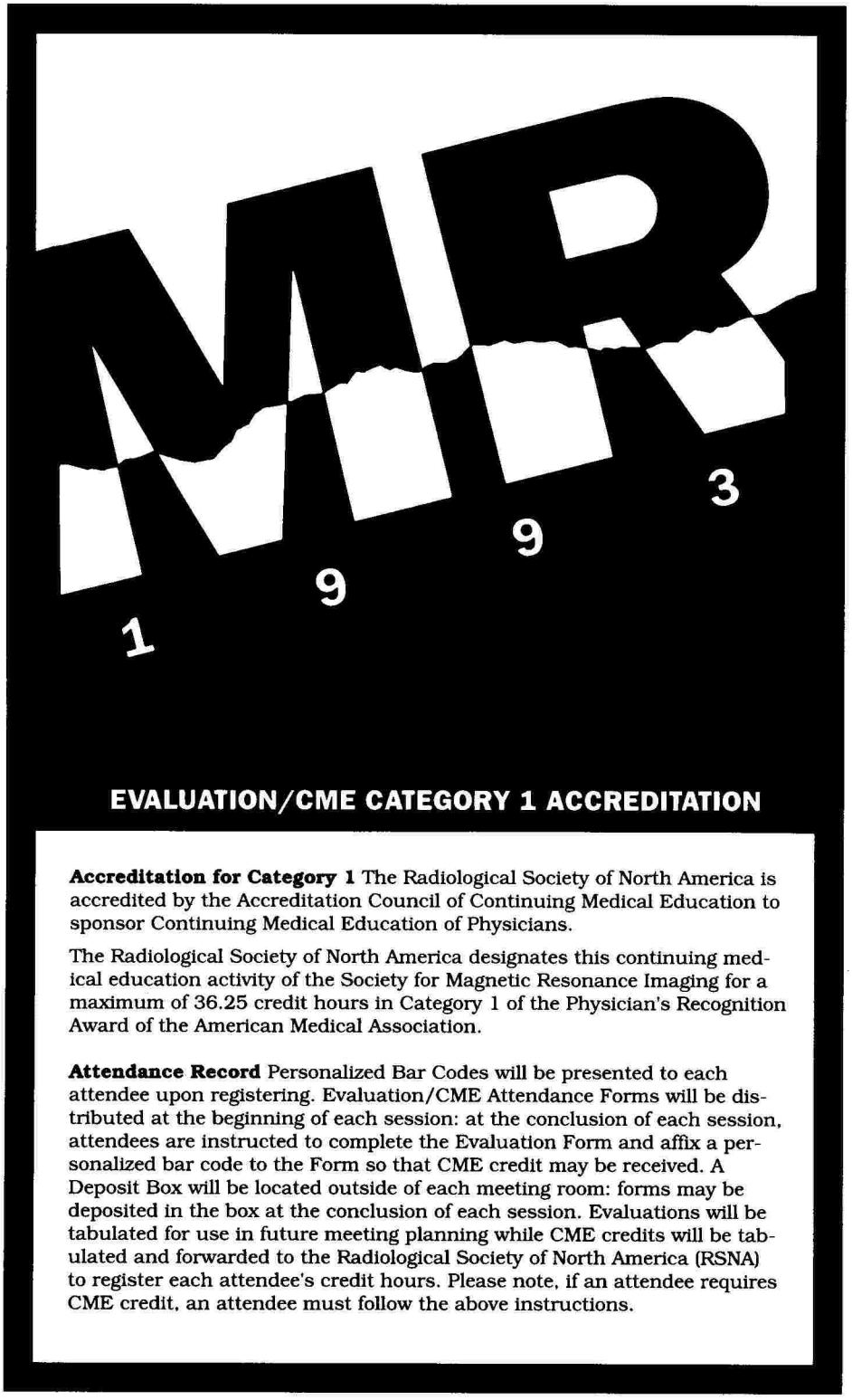

EVALUATION/CME CATEGORY 1 ACCREDITATION

Accreditation for Category 1 The Radiological Society of North America is accredited by the Accreditation Council of Continuing Medical Education to sponsor Continuing Medical Education of Physicians.

The Radiological Society of North America designates this continuing medical education activity of the Society for Magnetic Resonance Imaging for a maximum of 36.25 credit hours in Category 1 of the Physician's Recognition Award of the American Medical Association.

Attendance Record Personalized Bar Codes will be presented to each attendee upon registering. Evaluation/CME Attendance Forms will be distributed at the beginning of each session: at the conclusion of each session, attendees are instructed to complete the Evaluation Form and affix a personalized bar code to the Form so that CME credit may be received. A Deposit Box will be located outside of each meeting room: forms may be deposited in the box at the conclusion of each session. Evaluations will be tabulated for use in future meeting planning while CME credits will be tabulated and forwarded to the Radiological Society of North America (RSNA) to register each attendee's credit hours. Please note, if an attendee requires CME credit, an attendee must follow the above instructions.

DALLAS

SMRI

Society for Magnetic Resonance Imaging

MARCH 5-9, 1994

1994 ANNUAL MEETING

Future Meetings

1995 • March 25-29 • Washington, DC

1996 • April 20-26 • Vancouver, BC

SMRI

Society for Magnetic Resonance Imaging

213 West Institute Place
Suite 501
Chicago, IL 60610
312/751-2590